Missouri S&T
Library and
Learning Resources

Scholars' Mine

Doctoral Dissertations

Student Theses and Dissertations

Fall 2017

Node localization in underwater sensor networks (UWSN)

Huai Huang

Recommended Citation

NODE LOCALIZATION IN UNDERWATER SENSOR NETWORKS (UWSN)

by

HUAI HUANG

A DISSERTATION

Presented to the Graduate Faculty of the

MISSOURI UNIVERSITY OF SCIENCE AND TECHNOLOGY

In Partial Fulfillment of the Requirements for the Degree

DOCTOR OF PHILOSOPHY

in

ELECTRICAL ENGINEERING

2017

Approved by

Yahong Rosa Zheng, Advisor
Maciej J Zawodniok
Sahra Sedighsarvestani
Xiaoming He
Mohammad Ghasr

PUBLICATION DISSERTATION OPTION

This dissertation consists of the following four published or to be published papers, formatted in the style used by the Missouri University of Science and Technology, listed as follows:

Paper I, (pages 7–35) H. Huang, Y. R. Zheng, "3-D Localization of Wireless Sensor Nodes Using Near-Field Magnetic-Induction Communications", has been submitted to Elsevier Physical Communication, May. 2017.

Paper II, (pages 36–63) H. Huang, Y. R. Zheng, "Node Localization with AoA Assistance in Multi-hop Underwater Sensor Networks", has been submitted to Elsevier Ad Hoc Networks, Jun. 2017.

Paper III, (pages 64–79) H. Huang, Y. R. Zheng, "AoA Assisted Localization for Underwater Ad-Hoc Sensor Networks", has been accepted by MTS/IEEE OCEANS, Shanghai, China, Sep. 1-6, 2016.

Paper IV, (pages 80–95) H. Huang, Y. R. Zheng, "Pseudo-noise based time of arrival estimation for underwater acoustic sensor localization", has been accepted by MTS/IEEE OCEANS, Shanghai, China, Apr. 1-6, 2016.

ABSTRACT

This dissertation focuses on node localization in underwater wireless sensor networks (UWSNs) where anchor nodes have knowledge of their own locations and communicate with sensor nodes in acoustic or magnetic induction (MI) means. The sensor nodes utilize the communication signals and the locations of anchor nodes to locate themselves and propagate their locations through the network.

For UWSN using MI communications, this dissertation proposes two localization methods: rotation matrix (RM)-based method and the distance-based method. Both methods require only two anchor nodes with arbitrarily oriented tri-directional coils to locate one sensor node in the 3-D space, thus having advantages in a sparse network. Simulation studies show that the RM-based method achieves high localization accuracy, while the distance-based method exhibits less computational complexity.

For UWSN using acoustic communications, this dissertation proposes a novel multi-hop node localization method in the 2-D and 3-D spaces, respectively. The proposed method estimates Euclidean distances to anchor nodes via multi-hop propagations with the help of angle of arrival (AoA) measurements. Simulation results show that the proposed method achieves better localization accuracy than existing multi-hop methods, with high localization coverage.

This dissertation also investigates the hardware implementation of acoustic transmitter and receiver, and conducted field experiments with the hardware to estimate ToA using single pseudo-noise (PN) and dual PN(DPN) sequences. Both simulation and field test results show that the DPN sequences outperform the single PNs in severely dispersive channels and when the carrier frequency offset (CFO) is high.

ACKNOWLEDGMENTS

Firstly, I would like to thank my academic advisor Dr. Yahong Rosa Zheng. She has given me invaluable advice and guidance on my research during my Ph.D. study. Her acute insights and numerous experiences have always inspired me to explore new fields and overcome obstacles in my research. She has also given me a lot of suggestions on efficient task management, communication skills, and even career planning. She has provided me many good opportunities to attend conferences where I have broadened my horizons and improved my communication skills. Without her constructive guidance, insightful instructions, and generous financial support, this dissertation would have been impossible.

I would like to thank the members of my advisory committee, Dr. Sahra Sedighsarvestani, Dr. Xiaoming He, Dr. Maciej J Zawodniok, and Dr. Mohammad Ghasr for generously offering their time and advice for my research.

I would like to thank Dr. Yunfeng Han and Ming Yue for helping me to complete field experiments and hardware designs. I would like to thank Dr. Juening Jin for giving good advice and discussing about technique details of my research. I would like to thank all the current and previous members in the Communications and Real-Time Adaptive Signal Processing (CRASP) lab at Missouri S&T for their support and help on my study and life. I will cherish our friendship forever.

At last, I would like to thank my family for their unselfish love and unconditional support to me. I would like to thank my cat for accompanying me and warming my heart.

TABLE OF CONTENTS

SECTION

LIST OF ILLUSTRATIONS

LIST OF TABLES

1. INTRODUCTION

1.1. BACKGROUND

Underwater wireless sensor networks (UWSNs) have found important applications in ocean exploration, critical structure monitoring, coastal surveillance, motion tracking, and disaster mitigation [1]. In many applications of UWSNs, the position knowledge of wireless sensor nodes is desirable; otherwise, the sensing information collected is useless. The knowledge of geographic locations of nodes in a UWSN is typically required for mobility tracking, routing, and coordination purposes. Therefore, localization is a must-do task in many UWSN applications [2]. In UWSNs, anchor nodes have knowledge of their own locations and communicate with sensor nodes. The sensor nodes utilize the communication signals and the locations of anchor nodes to locate themselves and propagate their locations through the network, as shown in Fig. 1.1. The ratio of anchor nodes and the node degree of UWSN affect the localization coverage and accuracy. The recursive localization method is widely used in a network with relative high density. Conversely, multi-hop localization methods are feasible in a sparse network.

However, communication underwater is more challenging. Such environments impose various problems on traditional localization methods based on electromagnetic (EM) signals. The well-established EM-based global position system (GPS) is infeasible underwater since the EM signal attenuates dramatically with distance in water, which significantly limits the achievable communication range. Although people can prolong communication range by increasing antenna size or signal power, it costs more and is infeasible underwater. The widely used underwater localization is based on acoustic communications and reaches longer communication range. Fig. 1.2
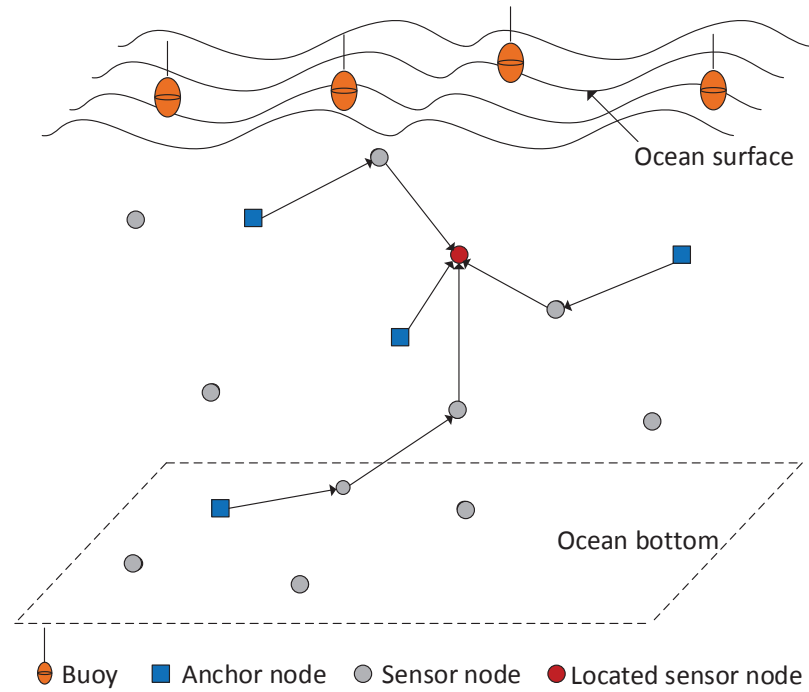
Figure 1.1. The framework of UWSN.

depicts the hardware of a transceiver node in UWSN based on acoustic communications, where Fig.1.2(a) shows a transducer that transmits and receives acoustic signals underwater, and Fig. 1.2(b) shows our designed circuit board that processes received data, with the dimension of 6 cm × 15 cm. This circuit board is mainly composed of amplifiers, filters, micro-controller unit (MCU), sensors, and power amplifier.

(a) Transducer
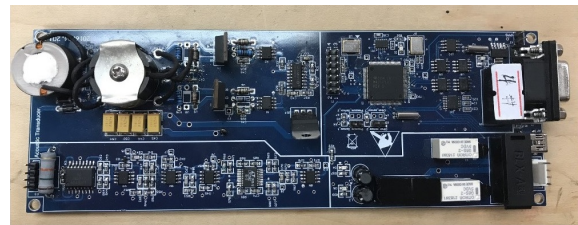
(b) Circuit board

Figure 1.2. Hardware on a transceiver node in acoustic communications.

Although acoustic communication underwater is common, it suffers from multipath fading caused by reflections from river bottom, water surface or obstacles, and Doppler effect caused by water flow or other motions nearby. Magnetic induction (MI) communication has become attractive in underwater or underground environments, where the light of sight is lacking and traditional communications encounter challenges. MI communications utilize magnetic field coupling produced by current loops in near-field to communicate. MI signal is immune to multi-path fading and the Doppler effect, and has high penetration. Besides, MI communications are implemented with low-cost and low power consumption. Fig. 1.3 depicts the hardware on a transceiver node in UWSN based on MI communications, where Fig.1.3(a) shows a tri-directional coil that couples magnetic field between nodes, and Fig. 1.3(b) shows our designed circuit board that processes received data, with the diameter of 6 cm. The input device on this circuit board is a watch-dog receiver chip AS3933 that has three inputs, each of which is connected to each coil of a tri-directional coil. Other main components on this board are MCU, sensors, and the transmitter chip ATA5276.
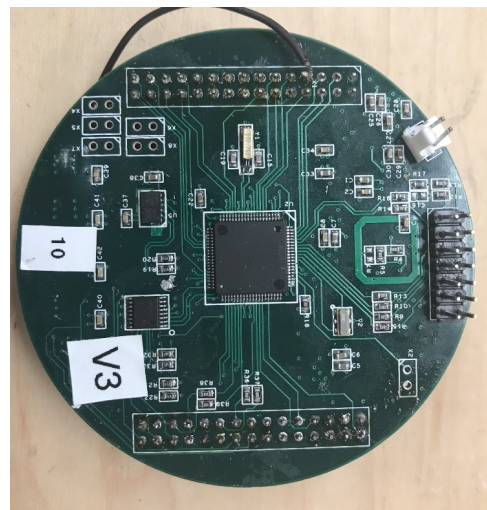
(a) Tri-directional coil   (b) Circuit board

Figure 1.3. Hardware on a transceiver node in MI communications.

1.2. PROBLEM STATEMENT

Localization usually has three phases: distance estimation, position estimation and refinement. Distance estimation is the foundation for a localization process, which is estimated via communications between nodes. The traditional localization schemes require at least three (in 2-D) or four (in 3-D) anchor nodes available to locate a sensor node by the trilateration algorithm. However, in a sparse large-scale wireless network, due to sensors moving and diffusing after deployment, there are some isolated nodes that cannot reach enough anchor nodes and thus are incapable of self-localization [3]. Some schemes have been developed to do localization in this case. AUV-aided algorithms use traveling AUVs to assist isolated nodes localization [4]. In a relatively dense network, the recursive localization method reaches high localization coverage [5]. However, when the network is sparse, the localization coverage decreases significantly because the recursive localization method requires at least four nodes (in 3-D) with awareness of positions around a to-locate sensor node. To extend the localization coverage in a sparse network, a category of localization schemes that are based on multi-hop distance propagation was proposed: DV-Hop, DV-Distance, and Euclidean method [6]. DV-Hop and DV-Distance methods can only reach coarse localization and are sensitive to anisotropic topologies. The Euclidean method achieves higher localization accuracy but much lower localization coverage. Multi-hop methods forward distance from anchor nodes to sensor nodes hop by hop. Once a sensor node gets distance estimations from at least four anchor nodes, the trilateration algorithm is employed to do localization. In recent years, some new multi-hop algorithms have been proposed to improve localization accuracy. Paper [7] uses the law of cosine to estimate distances from anchor nodes to sensor nodes. We call this the Cosine-law method. Paper [8] employs the greedy algorithm to find

the shortest path as the distance estimation, which is called as the Distance-based method. Our goal is to find a localization method that improves localization accuracy and keeps high localization coverage in a large-scale sparse network.

On the other hand, due to the promising features of MI communication over traditional communication technologies, MI-based localization has attracted a lot of interests. The major constraint on MI-based localization is the short range because the coupling of source and sensor coils used for MI communication must take place in the near-field, where $\lambda/2\pi >> R$ (λ is the wavelength and R is the transmission distance). Paper [9] proposes a method that completes localization only in 2-D coupled sensor networks. Paper [10] proposed a method that completes localization in the 3-D space, using beacons of low-frequency magnetic field, which requires the source coils to face the fixed axes exactly, and the sensor coils have to face the source coils exactly. In practice, it is difficult to fix the orientations of coils and the orientations might change with water flow. This dissertation proposes two MI-based localization method that completes localization of nodes with arbitrary position and orientation after deployment in both 2-D and 3-D spaces.

1.3. SUMMARY OF CONTRIBUTIONS

This dissertation consists of a couple of journal publications and conference papers listed in the publication list. My contributions that are published or under review are:

1. For UWSN using MI communications, this dissertation proposes two localization methods: rotation matrix (RM)-based method and the distance-based method. Both methods require only two anchor nodes with arbitrarily oriented tri-directional coils to locate one sensor node in the 3-D space, thus having advantages in

a sparse network. Simulation studies show that the RM-based method achieves high localization accuracy, while the distance-based method exhibits less computational complexity.

2. For UWSN using acoustic communications, this dissertation proposes a novel multi-hop node localization method in the 2-D and 3-D spaces, respectively. The proposed method estimates Euclidean distances to anchor nodes via multi-hop propagations with the help of angle of arrival (AoA) measurements. A weighted least square method that adjusts weights based on the number of hops is used to improve localization accuracy further. Simulation results show that the proposed method achieves better localization accuracy than existing multi-hop methods. Additionally, the proposed method still keeps high localization coverage.

3. This dissertation also investigates the hardware implementation of acoustic transmitter and receiver, and conducted field experiments with the hardware to estimate ToA using single pseudo-noise (PN) and dual PN(DPN) sequences. Both simulation and field test results show that the DPN sequences outperform the single PNs in severely dispersive channels and when the carrier frequency offset (CFO) is high in low-cost hardware systems where the atomic clock is unavailable.

PAPER

I. 3-D LOCALIZATION OF WIRELESS SENSOR NODES USING NEAR-FIELD MAGNETIC-INDUCTION COMMUNICATIONS

Huai Huang and Yahong Rosa Zheng

Department of Electrical & Computer Engineering

Missouri University of Science and Technology

Rolla, Missouri 65409–0050

Email: {hh6v8, zhengyr}@mst.edu

ABSTRACT

This paper proposes two localization methods for wireless sensor nodes that utilize an arbitrarily oriented tri-directional coils in magnetic induction (MI) transceivers. Taking advantage of magnetic field measurements of a tri-directional coil antenna in the near-field, the two localization algorithms use only two anchor nodes to locate a sensor node in the 3-D space. Assuming each anchor node transmits the communication signals by three coils sequentially, which are received by the three coils at a sensor node simultaneously, this paper derives closed-form formulas for estimating the transmission distance and the polar angles to yield 8 possible location points based on the signals of each anchor node. Then a rotation matrix (RM)-based method derives the orientation rotation matrix between the transmitter and receiver to find out two possible location vectors with the opposite directions in each anchor node. Then, we use maximum likelihood to estimate the location with two anchor nodes assisted. Another method called the Distance-based method, taking the locations of the two

anchor nodes and the two sets of 8 possible location estimates of the sensor node, estimates the location by minimizing the distance. The RM-based method can achieve high localization accuracy while the distance-based method has less computational complexity. However, the Distance-based method may encounter location ambiguity when the orientations of the two anchor nodes are the same. Simulations are performed to compare these two algorithms and the existing localization algorithm in this scenario. The results show that the proposed two localization algorithms and the derived closed-form formula of distance achieve good accuracy under large measurement errors.

1. INTRODUCTION

Magnetic induction (MI) communication has been developed for wireless communication in challenging environments, such as underwater and underground, where traditional Radio Frequency (RF) communication technologies encounter formidable difficulties [1, 2]. The advantages of MI communications are low cost, negligible propagation delay, no multipath interference, no requirement of line of sight. The limitations of MI communications include small bandwidth, severe range attenuation, and strong directionality of antenna coils. With short range and low data rate, MI communication has been applied to underwater or underground wireless sensor networks (UWSN), which in turn find important applications [3] in underground structure monitoring, earthquake and landslide prediction, bridge scour monitoring, river bank monitoring, landscape management, and border patrol and security, etc.

An important task of UWSNs is the localization of sensor nodes in the network because it is often desirable to collect sensing data associated with position information. The knowledge of geographic positions of nodes is also required for mobility tracking, routing, and coordination purposes. Indoor robot navigation is

reported in [4, 5, 6, 7, 8]; underground target localization and tracking are reported in [7, 9, 10, 11, 12]; and tracking medicine application in human bodies is reported in [13, 14].

Typically, a node localizes itself by communicating with other nodes around it. In a wireless sensor network, a node whose absolute location is known to all nodes is termed as an *anchor* node whose location is used as a reference in the global coordinate system (GCS). The other ordinary nodes are called *sensor* nodes which have to estimate their own locations. Taking advantage of the knowledge of anchor nodes and communications between nodes, the locations of sensor nodes are usually estimated via tri-lateralization or triangularization if the sensor node can communicate with three or more anchor nodes [15]. In a dense network, if the percentage of anchor nodes is small, then the recursive position estimation method [16, 17] is commonly used to cover the whole network of sensor nodes.

On the other hand, in sparse wireless sensor networks where the node degree is very small due to limitations in communication range, as often the case in MI sensor networks, the localization of sensor nodes faces many technical challenges because the number of neighboring nodes is often less than three and the percentage of anchor nodes can be very small. The directionality of MI coils also causes ambiguity in range estimation if the orientations of the transmitter and receiver coils are unknown because the received signal strength indicator is affected by the range as well as the coil orientations [7, 18, 19, 20, 2]. Besides, a magnetic field is easy to be interfered by metals nearby and the earth's geomagnetic field, causing localization errors [21, 22, 23, 24].

Remedies to the challenges of MI sensor localization include: 1) in special environments such as pipeline systems and indoor environment, coil orientations are constrained to a fixed known direction [25, 26, 27] and range estimation is obtained with RSSI measurements; 2) localization is constrained to a 2-D plane [28] by using

input impedance measurements at several reference nodes; 3) orientation sensors are used in addition to communication signals to aid the range estimation, as reported in [29]; 4) large coils are arranged in a 2-D plane to form a magnetic grid, then the received signals on these large coils are estimated to find the coarse locations of the transmitter [7]. All these methods suffer from stringent constraints, inflexible implementation or high localization errors.

In this paper, we propose two novel methods for MI sensor localization in 3-D space using only two anchor nodes and their communication signals with the sensor node. All nodes can have arbitrary orientations and positions in the 3-D space, and they all employ tri-directional coil antennas for MI communication. By taking advantage of the directionality of the three orthogonal transmitting (source) coils at each of the two anchor nodes, the sensor node, also equipped with a tri-directional coil that is receiving (sensor) coils, can estimate its transmission distance to the anchor nodes without ambiguity, and can estimate two possible polar angles for each transmitting coil. This results in two sets of 8 possible location estimates for the sensor node. Rotation matrix (RM)-based method uses 8 location estimates to compute the rotation matrix between the transmitting and receiving coils and identify one pair of diagonal points with the opposite directions in each anchor node, and then utilizes maximum likelihood and gradient ascent algorithm to estimate the sensor node location. RM-based method yields high localization accuracy under measurement errors. The distance-based method uses the minimal distance rule to select the best pair of location estimates from the two sets of 8 points, and determines its location by Minimum mean-square error (MMSE) estimation. This method has less computational complexity and is faster but may encounter estimation ambiguity when the two anchor nodes have the same orientation. This localization ambiguity can be solved by the RM-based method. Through computer simulations, we verify that the two methods work well even if large errors exist in measurements.

2. BACKGROUND

Assume that the anchor nodes and sensor nodes are equipped with tri-directional coil antennas, as shown in Fig. 1, where the three coils are orthogonal to each other and their centers are co-located. Let R be the distance between node S and the center of the coils. The local coordinate system (LCS) of the anchor node is defined with the x, y, and z axes aligned with the axes of the three coils, respectively. The three coils are excited sequentially by a current source $i(t) = I \exp\{j\omega t\}$ with $j = \sqrt{-1}$, each of which produces an magnetic flux density at the sensor node location S.
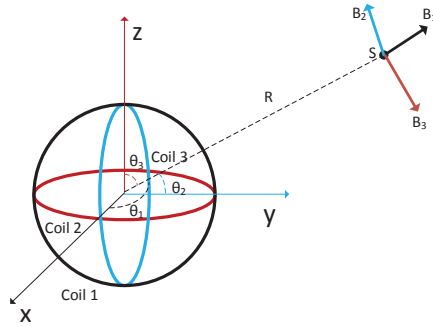
Figure 1. Magnetic field generated by a source tri-directional coil.

Let $\mathbf{B}_k$ be the magnetic flux density at S generated by the kth transmitting coil, and θ_k be the polar angle of S against the x, y, z axis, respectively, where $k = 1, 2,$ and 3. If the distance R is more than four times of the radius r of the coil, the magnetic field produced by the current loop is equivalent to that from a magnetic dipole. In other words, the source and sensor coils can be treated as single points [30]. Hence, the magnetic flux density $\mathbf{B}_k$ at node S only depends on the distance R and the polar angles θ_k as

$$\mathbf{B}_k = \begin{cases} B_{kr} = (M\mu/2\pi R^3)\cos(\theta_k) \\ \\ B_{kt} = (M\mu/4\pi R^3)\sin(\theta_k) \end{cases} \quad (1)$$

where the subscripts r and t denote the radial and tangential components of the magnetic flux density $\mathbf{B}_k$, respectively, M is the magnitude of magnetic moment $\mathbf{M}$ of the current loop and μ is the magnetic permeability of the medium. The equation (1) holds for the magnetic field of a coil in the near-field. For more general expression of a magnetic field induced along a closed curve, please refer to the Biot-Savart law [21].

The magnetic moment $\mathbf{M}$ is calculated by

$$\mathbf{M} = NIA\vec{\mathbf{F}} \tag{2}$$

where N and A are the number of coil turns and the area of the current coil, respectively. Although the excitation current $i(t)$ depends on the carrier frequency ω, the amplitude of the magnetic field is independent of ω. The unit vector $\vec{\mathbf{F}}$ denotes the axis of the coil which is perpendicular to the coil plane and follows the right-hand rule. We also note that the spatial phase variation of $\exp(jR/\lambda)$ can be ignored as long as the coil is in the near-field or quasi-static field that satisfies $\lambda/2\pi >> R$, where λ is the wavelength. Therefore, the magnitude of the magnetic flux density $\mathbf{B}_k$ is expressed as

$$B_k = \sqrt{B_{kr}^2 + B_{kt}^2} \tag{3}$$

At the sensor receiver, the magnitude B_k of the magnetic field of the kth transmitting coil is measured by three receiving coils as

$$B_k = \sqrt{B_{k1}^2 + B_{k2}^2 + B_{k3}^2} \tag{4}$$

where the subscripts 1, 2 and 3 represent three orthogonal coils at the receiver side [7]. By using (4), the magnitude of magnetic flux density is measured invariant to the orientation of the sensor coils, which has the advantage that the sensor nodes can have an arbitrary orientation.

3. THE PROPOSED LOCALIZATION SCHEMES

In this section, we propose two MI-based localization algorithms in the near-field. We try to locate sensor nodes, based on the measured magnetic flux density, the known spatial geometry dimensions of the coils, and the prior knowledge of locations and orientations of two anchor nodes.

3.1. Transmission distance and polar angles. First, we estimate the transmission distance between source coils and sensor coils. According to (3), the magnitude B_k satisfies

$$B_k^2 = B_{kr}^2 + B_{kt}^2 \tag{5}$$

Substituting (1) into (5) yields

$$
\begin{aligned}
B_k^2 &= \frac{C_k^2}{R^6} \cos^2 \theta_k + \frac{1}{4} \frac{C_k^2}{R^6} \sin^2 \theta_k \\
&= \frac{3}{4} \frac{C_k^2}{R^6} \cos^2 \theta_k + \frac{1}{4} \frac{C_k^2}{R^6}
\end{aligned}
\tag{6}
$$

where $C_k = \frac{\mu M_k}{2\pi}$. Therefore, once B_k is measured, the corresponding polar angle θ_k is calculated by

$$\cos^2 \theta_k = \frac{4R^6 B_k^2 - C_k^2}{3C_k^2} \tag{7}$$

The three polar angles of the vector S in the local Cartesian coordinate system satisfy

$$\cos^2 \theta_1 + \cos^2 \theta_2 + \cos^2 \theta_3 = 1 \tag{8}$$

Substituting (7) into (8), we have

$$\sum_{k=1}^{3} \frac{4R^6 B_k^2 - C_k^2}{3C_k^2} = 1.$$ (9)

Consequently, the distance R is calculated by

$$R = \left(\frac{3}{2 \sum_{k=1}^{3} \frac{B_k^2}{C_k^2}} \right)^{\frac{1}{6}}$$ (10)

Substituting (10) to (7), the polar angle θ_k is obtained.

When all three transmitting coils have the same magnitude of the magnetic moment, or $M_k = M$, then $C_k = C$. In this case, the computation of the distance R in (10) is simplified as

$$R = \left(\frac{3C^2}{2 \sum_{k=1}^{3} B_k^2} \right)^{\frac{1}{6}}$$ (11)

Let $B_{rms} = \sqrt{\sum_{k=1}^{3} B_k^2}$, then R is

$$R = \left(\frac{3}{2} \right)^{\frac{1}{6}} \left(\frac{C}{B_{rms}} \right)^{\frac{1}{3}}$$ (12)

The polar angles θ_k can be computed from (7) and (12) and each of them has two possible solutions

$$\theta_k = \arccos \sqrt{\frac{6B_k^2 - B_{rms}^2}{3B_{rms}^2}}$$
$$or \quad \theta_k = \pi - \arccos \sqrt{\frac{6B_k^2 - B_{rms}^2}{3B_{rms}^2}}$$ (13)

for $\theta_k \in [0, \pi]$. However, with noise and measurement errors considered, the right side of equation (7) might be less than 0 or larger than 1, which causes (13) has no correct solution. In this case, we optimize measured B_k to make the value of (7) be

within the limits of 0 and 1. Substituting (12) to (7), each B_k must satisfies

$$\frac{1}{6}B_{rms}^2 \leq B_k^2 \leq \frac{2}{3}B_{rms}^2 \tag{14}$$

Once B_k is beyond the range of (14) caused by noise or measurement errors, we optimize B_k by

$$\begin{aligned} \text{minimize} \quad & ||\hat{\mathbf{B}}^2 - \mathbf{B}^2||_2 \\ \text{subject to} \quad & \frac{1}{6}B_{rms}^2 \leq \hat{B}_k^2 \leq \frac{2}{3}B_{rms}^2 \end{aligned} \tag{15}$$

where $\hat{\mathbf{B}}^2 = [\hat{B}_1^2, \hat{B}_2^2, \hat{B}_3^2]^T$ and $\mathbf{B}^2 = [B_1^2, B_2^2, B_3^2]^T$. We define a matrix $\mathbf{E}$ of dimension 6×3 as,

$$\mathbf{E} = \left[\frac{1}{6}\mathbf{K} - \mathbf{I}; \mathbf{I} - \frac{2}{3}\mathbf{K}\right] \tag{16}$$

where $\mathbf{K}$ is an all-ones matrix of dimension 3×3, $\mathbf{I}$ denotes the identity matrix of dimension 3×3. The constraint in (15) can be reformulated as

$$\mathbf{E}\hat{\mathbf{B}}^2 \leq 0 \tag{17}$$

By utilizing the *logarithmic barrier* method in [31], the optimal solution of (15) can be obtained.

The direction of the position vector, which is termed as *bearing versor* $\boldsymbol{\nu}$, is calculated by

$$\boldsymbol{\nu} = [\cos\theta_1, \cos\theta_2, \cos\theta_3]^T \tag{18}$$

Since each $\cos\theta_k$ has two possible signs, the bearing versor has 8 possible solutions, each of which is termed as $\boldsymbol{\nu}_{ln}$, where l is the anchor node index, and $n = 1, \cdots, 8$. Hence, there are 8 corresponding location points $\mathbf{S}'_{ln}$ in each LCS.

$$\mathbf{S}'_{ln} = R_l \boldsymbol{\nu}_{ln} \tag{19}$$

To identify the true location of the sensor node out of the 8 possible points, we utilize another anchor node A_2, which has arbitrary orientation and position, as shown in Fig. 2. When the tri-directional coil antennas of anchor nodes A_1 and A_2 have different orientations, the LCSs $x_1 y_1 z_1$ and $x_2 y_2 z_2$ are differently oriented. With the same method as in (11) and (13), another set of 8 possible location points is obtained in the LCS of A_2. The two sets of 8 points are denoted as $\mathbf{S}'_{ln} = [x'_{ln}, y'_{ln}, z'_{ln}]^T$, where $l = 1, 2$, marked as the small circles and stars in Fig. 2, where coordinate system XYZ
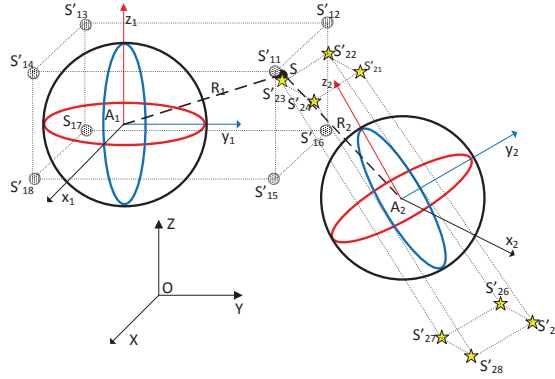
Figure 2. Localization by two tri-directional coil antennas in 3-D.

is the GCS. The absolute coordinates of the two anchor nodes A_1 and A_2 in the GCS are known from GPS or other survey systems, and we assume their orientations can be measured by inclination sensors and determined by calibration.

With the 16 possible candidate locations of the sensor node, we propose two schemes to estimate the true location S of the sensor node in Fig. 2.

3.2. Rotation matrix (RM)-based method. The excitation of a source tri-directional coil and the sensor tri-directional coil output are most conveniently described in vector notion. Let vector $\mathbf{g}_t$ is the excitation vector of a source tri-directional coil and $\mathbf{g}_r$ be the coupled magnetic field vector of the sensor tri-directional coil.

Table 1. Orthogonal rotation matrices

	Postion				Orientation		
Azimuth rotates X into Y	$Q_\vartheta =$	$\begin{array}{ccc}\cos\vartheta & \sin\vartheta & 0 \\ -\sin\vartheta & \cos\vartheta & 0 \\ 0 & 0 & 1\end{array}$		$Q_\alpha =$	$\begin{array}{ccc}\cos\alpha & \sin\alpha & 0 \\ -\sin\alpha & \cos\alpha & 0 \\ 0 & 0 & 1\end{array}$		
Elevation rotates X into -Z	$Q_\psi =$	$\begin{array}{ccc}\cos\psi & 0 & -\sin\psi \\ 0 & 1 & 0 \\ \sin\psi & 0 & \cos\psi\end{array}$		$Q_\beta =$	$\begin{array}{ccc}\cos\beta & 0 & -\sin\beta \\ 0 & 1 & 0 \\ \sin\beta & 0 & \cos\beta\end{array}$		
Roll rotates Y into Z	$Q_\phi =$	$\begin{array}{ccc}1 & 0 & 0 \\ 0 & \cos\phi & \sin\phi \\ 0 & -\sin\phi & \cos\phi\end{array}$		$Q_\gamma =$	$\begin{array}{ccc}1 & 0 & 0 \\ 0 & \cos\gamma & \sin\gamma \\ 0 & -\sin\gamma & \cos\gamma\end{array}$		

If the round number, the geometry size and excitation current of the three transmitting coils are identical and they are excited simultaneously, the excitation vector of a source tri-directional coil can be expressed as $\mathbf{g}_t = [C, C, C]^T$, where $C = NIA\mu/2\pi$.

Since the three transmitting coils are excited sequentially, only one coil is active while the other two are inactive at one time. Hence, the source vector $\mathbf{g}_t$ is expressed as $[C, 0, 0]^T$ when the coil facing to axis x is working, as $[0, C, 0]^T$ when the coil facing to axis y is working, and as $[0, 0, C]^T$ when the coil facing to axis z is working. The three vectors form a source matrix $\mathbf{G}_t$ expressed as

$$\mathbf{G}_t = C \begin{bmatrix} 1 & 0 & 0 \\ 0 & 1 & 0 \\ 0 & 0 & 1 \end{bmatrix} = C\mathbf{I} \tag{20}$$

The three sensor coils are receiving at the same time. For each transmitting coil, there is a vector output of three resultant magnetic field measurements. Therefore, we totally have nine output measurements at the sensor node, which form a sensor matrix $\mathbf{G}_r$ expressed by

$$\mathbf{G}_r = \begin{bmatrix} B_{11} & B_{21} & B_{31} \\ B_{12} & B_{22} & B_{32} \\ B_{13} & B_{23} & B_{33} \end{bmatrix} \tag{21}$$

where each column corresponds to a transmitting coil. According to the coupling of source and sensor coils presented in paper [30], we have

$$\mathbf{G}_r = \frac{1}{R^3}\mathbf{\Gamma}\mathbf{P}\mathbf{G}_t = \frac{C}{R^3}\mathbf{\Gamma}\mathbf{P} \tag{22}$$

where matrix $\mathbf{\Gamma}$ is the rotation matrix between the source tri-directional coil and the sensor tri-directional coil, and matrix $\mathbf{P}$ denotes the position impact. Matrix $\mathbf{\Gamma}$ is calculated by

$$\mathbf{\Gamma} = Q_\alpha Q_\beta Q_\gamma \tag{23}$$

where Q_α, Q_β, and Q_γ are orientation rotation matrices defined in Table 1. Matrix $\mathbf{P}$ is calculated by

$$\mathbf{P} = Q_{-\psi}Q_{-\vartheta}\mathbf{V}Q_\vartheta Q_\psi \tag{24}$$

where Q_ψ and Q_ϑ are position rotation matrices defined in Table 1, and matrix $\mathbf{V}$ is defined as

$$\mathbf{V} = \begin{bmatrix} 1 & 0 & 0 \\ 0 & -\frac{1}{2} & 0 \\ 0 & 0 & -\frac{1}{2} \end{bmatrix} \tag{25}$$

An anchor node provides 8 possible location points, each of which locates in a quadrant of the LCS. From (24), the 8 possible locations generate 8 different matrices $\mathbf{P}_n$. Then, 8 corresponding matrices $\mathbf{\Gamma}_n$ are calculated by

$$\mathbf{\Gamma}_n = \frac{R^3}{C}\mathbf{G}_r\mathbf{P}_n^{-1} \qquad n = 1, 2...8 \tag{26}$$

Since matrix $\mathbf{\Gamma}_n$ is expected to be a rotation matrix, i.e., $\mathbf{\Gamma}_n\mathbf{\Gamma}_n^T = \mathbf{I}$. However, the matrix $\mathbf{P}_n$ might not be calculated by the true location of the sensor node S, resulting in the corresponding matrix $\mathbf{\Gamma}_n$ might not satisfy the property of a rotation matrix. Due to the symmetry of the magnetic field, two of the 8 matrices $\mathbf{\Gamma}_n$ are rotation

matrices, the two corresponding location points of which are located in two diagonal quadrants. One of the two points is the true location and the other one is in its diagonal quadrant with the opposite direction. Therefor, one anchor node provides a pair of location points with opposite bearing versors. Two anchor nodes provides two sets of such diagonal points. For example, in Fig. 2, points S'_{11} and S'_{17}, points S'_{23} and S'_{25} are the two sets of diagonal points with the opposite directions.

We should pay attention to that with measurement errors or noise considered, we cannot determine if the matrix $\boldsymbol{\Gamma}_n$ is a rotation matrix based on $\boldsymbol{\Gamma}_n\boldsymbol{\Gamma}_n^T = \mathbf{I}$, because $\boldsymbol{\Gamma}_n$ is not an exact rotation matrix even for the true location point. The matrix $\boldsymbol{\Gamma}_n$ of the true location point is similar to a rotation matrix, but corrupted by measurement errors or noise. To evaluate the similarity between matrix $\boldsymbol{\Gamma}_n$ and an ideal rotation matrix, we do singular value decomposition (SVD) of matrix $\boldsymbol{\Gamma}_n$ as

$$\boldsymbol{\Gamma}_n = \mathbf{U}\boldsymbol{\Sigma}\mathbf{V}^* \tag{27}$$

where $\mathbf{U}$ and $\mathbf{V}^*$ are rotation matrices, $()^*$ is the conjugate transpose of a matrix, and $\boldsymbol{\Sigma}$ is a diagonal matrix with the singular values as the diagonal elements. We define H_n as

$$H_n = \|\mathbf{I} - \boldsymbol{\Sigma}\|_2 \tag{28}$$

The smaller H_n is, the closer the matrix $\boldsymbol{\Gamma}_n$ is to an ideal rotation matrix. When $\boldsymbol{\Gamma}_n$ is an exact rotation matrix, $H_n = 0$. Therefore, we find two matrices $\boldsymbol{\Gamma}_n$ with the least H_n to get the corresponding two possible location points in a LCS.

Once the two sets of two location points with opposite directions in two LCSs are obtained, we utilize the maximum *log-likelihood* used in [32] to find out the location estimation.

1) Distance likelihood: We assume the estimated distance R_l follows Gaussian distribution with the estimated value from (12) as the mean value and $\sigma_{R,l}$ as the standard deviation. Therefore, the distance log-likelihood function of distance is calculated by

$$L_R(S) = c_1 - \sum_{l=1}^{2} \frac{1}{2\sigma_{R,l}^2}(\|S - A_l\|_2 - R_l)^2 \tag{29}$$

where S is the location of the sensor node, R_l is calculated by (12) in each LCS, c_1 is a constant that is independent of location S, and A_l is the absolute coordinates of anchor node A_l in the GCS.

2) Bearing versor likelihood: According to paper [32], we use Mises-Fisher distribution to describe the probability density of the bearing versor. The log-likelihood function of direction of location S is expressed as

$$L_D(S) = c_2 + \sum_{l=1}^{2} \ln \cosh \left(\chi_l \frac{(S - A_l)^T (S_{ln} - A_l)}{\|S - A_l\|_2 \|S_{ln} - A_l\|_2} \right) \tag{30}$$

where S_{ln} is the location in GCS of chosen location points according to (28), which is calculated by (34), χ_l is the concentration parameter and defined in paper [32], and c_2 is a constant that is independent of location S.

Therefore, the overall join log-likelihood of distance and direction is

$$L(S) = L_R(S) + L_D(S) \tag{31}$$

Our goal is to find the location S that makes (31) to reach the maximum value. The likelihood achieves the maximum value at location S by gradient ascent. The location estimation at the mth iteration is calculated by

$$S^{(m)} = S^{(m-1)} + \tau \frac{dL(S)}{dS}\Big|_{S=S^{(m-1)}} \tag{32}$$

where τ is the step size and $\frac{dL(S)}{dS}|_{S=S^{(m-1)}}$ is the gradient of $L(S)$ at the m-1 iteration. The gradient is calculated by

$$
\begin{aligned}
\frac{dL(S)}{dS} =& \sum_{l=1}^{2} \frac{(\|S - A_l\|_2 - R_l)(S - A_l)}{\sigma_{R,l}^2 \|S - A_l\|_2} \\
&+ \sum_{l=1}^{2} \left[\chi_l \frac{(S - A_L)^T (S_{ln} - A_l)}{\|S - A_l\|_2 (S_{ln} - A_l)} \right] \\
&\times \chi_l \left[\frac{1}{\|S - A_l\|_2} \mathbf{I} - \frac{(S - A_l)(S - A_l)^T}{\|S - A_l\|_2^3} \right] \\
&\times \left[\frac{(S_{ln} - A_l)}{(S_{ln} - A_l)} \right]
\end{aligned}
\tag{33}
$$

By using *Backtracking line search* in [31], we control the step size τ and the converge direction of each iteration to get the optimal solution. However, since the likelihood $L(S)$ is not convex, it is possible that (32) converges at a location that doesn't reach the maximum likelihood. In this case, the localization error would be bigger. To eliminate this possibility, we need to select the initial values of S, instead of randomly generated. If the initial value of S is close to the real location S, it is more likely to converge at the location with the maximum likelihood. Hence, we sequentially set the initial value equals to S_{1n}, $-S_{1n}$, $S_{2n'}$, and $-S_{2n'}$ to find the location that has the maximum likelihood.

3.3. Distance-based method. We transform the 16 coordinates in two LCSs into the GCS by

$$
S_{ln} = Q_l S'_{ln} + A_l \qquad n = 1, 2, \cdots, 8, \quad l = 1, 2
\tag{34}
$$

where Q_l is the rotation matrix between the LCS of node A_l and the GCS. The rotation matrix Q_l is determined by the orientation of the LCS which can be measured by inclination sensors. Once coordinates of the sixteen points in the GCS are obtained, we are able to calculate the pairwise distance of nodes from two LCSs and find the pair

of points (S^*_{1n} and $S^*_{2n'}$) that has the minimal distance between them by brute-force search in (35).

$$\underset{n,n'}{\operatorname{argmin}} \|S_{1n} - S_{2n'}\| \tag{35}$$

The two points with the minimal distance are considered as the pair of points that overlap. The estimated location of the sensor node S is obtained via MMSE estimation by

$$\underset{S}{\operatorname{argmin}} (\|S - S^*_{1n}\|^2 + \|S - S^*_{2n'}\|^2) \tag{36}$$

And (7) can be estimated by

$$S = \frac{S^*_{1n} + S^*_{2n'}}{2} \tag{37}$$

In (37), we consider the two anchor nodes have the same weight at estimating the location. However, each anchor node might has different measurement errors, noise, and location, resulting in different impacts on location estimation. In this paper, we assign different weight to each anchor nodes according to the transmission distance. From (6), since the transmission distance satisfies $B_k \propto R^{-6}$, we define weight on an anchor node A_l as

$$W_l = \frac{R_l^{-6}}{\sum_1^2 R_i^{-6}} \tag{38}$$

where R_i and R_l are transmission distances calculated by (12). Once weight W_l is gotten, (37) is modified as

$$S = \sum_{l=1}^{2} W_l S^*_{ln} \tag{39}$$

where subscript n is changed corresponding to different l.

The distance-based method has less computational complexity and is faster. However, it encounters localization ambiguity in the cases shown in Fig. 3, where the two LCSs have the same orientation. If the line-of-sight of the two anchor nodes aligns with one of the three axes, there are four pairs of points that are located in a plane overlap without considering errors or noise. For example, in Fig. 3(a), the line

of $A_1 A_2$ aligns with the axis y_1 or axis y_2. The points S'_{11} and S'_{24}, S'_{12} and S'_{23}, S'_{15} and S'_{28}, S'_{16} and S'_{27} overlap. In this case, we are incapable of identifying the true location of the sensor node by finding the minimal distance. In other words, there is localization ambiguity or the localization error would be large in this case.

Another case of localization ambiguity is that the anchor nodes A_1 and A_2 are located on a plane that is perpendicular to one of the three axes, as shown in Fig. 3(b). There are two pairs of points that overlap without considering measurement errors, such as points S'_{11} and S'_{23}, and points S'_{15} and S'_{27} in Fig. 3(b). Therefore, this situation also results in localization ambiguity. On the other hand, the RM-based method can solve the localization ambiguity, since there are only two possible position vectors with the opposite bearing versors in each LCS.

(a) case 1   (b) case 2
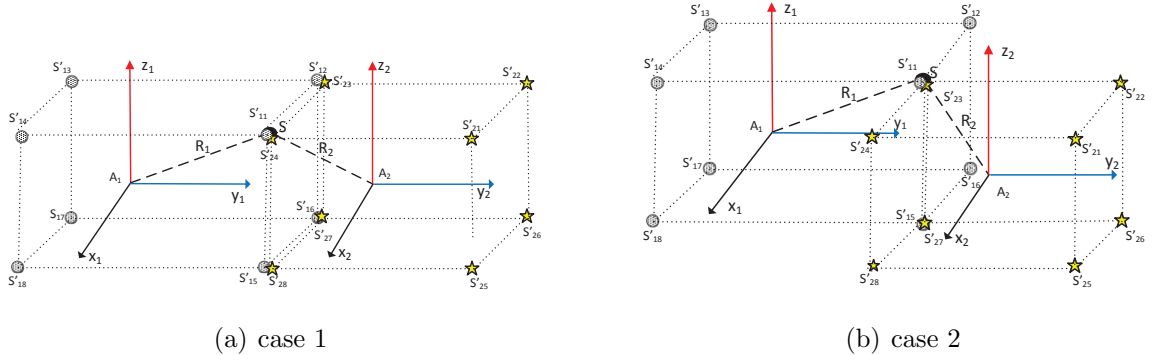
Figure 3. Localization ambiguity in two special cases

Since the absolute coordinates and the orientation of anchor nodes can be obtained from GPS and inclination sensors, respectively, it is easy to determine if the scenario of anchor nodes results in localization ambiguity in Fig. 3. We can adopt the RM-based method in this case.

Table 2. Parameters used in simulations.

Parameter	Value
Space size D	20 m
# of coil turns	50
Excitation current I	1 A
Coil radius r	17.8 cm

4. PERFORMANCE EVALUATION

The performances of the proposed localization methods are evaluated by computer simulations. The anchor nodes and sensor nodes are randomly placed in a $D \times D \times D$ space. The parameters for simulations are specified in Table 2.

4.1. Transmission distance. In this paper, we derived a closed-form formula of transmission distance based on magnetic flux density. The measurement of the magnetic flux density is influenced by various factors, such as metals nearby, geomagnetic field, and rocks [33]. The errors in paper [34] are modeled by the Gaussian mixture model. In this paper, we assume the measurement errors of the magnetic flux density follows the normal distribution, with zeros mean and σ_B as the standard deviations. RSSI model is wide used to estimate distance [32]. Fig. 4 depicts the distance errors of our method and the RSSI-based method, which is normalized by space size D. In our simulations, we assume the reference distance used in RSSI model has no error. Our method achieves smaller distance error with various σ_B.

4.2. Localization accuracy. To verify the two localization algorithms, we assume no measurement errors or noise in the simulations. The simulation results of the localization error ϵ, which is defined as the Euclidean distance between the estimated and the true locations of sensor nodes. The localization error is normalized by the space dimension D. We see that the localization errors are small enough to be considered as round-off errors from simulation software, no measurement errors or noise considered. Therefore, both of the two localization schemes are valid.
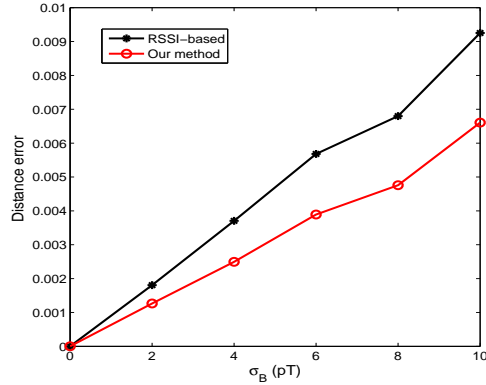
Figure 4. Distancce errors with various σ_B (magnetic flux density).

The two localization methods are based on the measurements of magnetic flux density, which influence the distance estimation R between source coils and sensor coils and polar angle estimations. Hence, the measurement error of the magnetic flux density is a major factor that affects the localization accuracy.

The localization method in paper [32] uses maximum eigenvector to find the bearing versor, which we call *Eigenvector-based* method. Once the bearing versor and distance are obtained, at least two anchor nodes are required to get localization without ambiguity. Then, Maximum log-likelihood and gradient ascent algorithm are employed to estimate the location from four possible position vectors. Although paper [32] implements localization in a network with multiple anchor nodes, in our simulations only two anchor nodes are used. By simulations, we find that the initial value of location S in (33) is critical. The Eigenvector-based method with random initial S is called Eigenvector-based 1. We also apply our selection rule of the initial value to the Eigenvector-based method, which is called Eigenvector-based 2. The average localization errors normalized by the space dimension D with various σ_B are shown in Fig. 5. From the results, RM-based method outperforms Distance-based

method and slightly underperforms Eigenvector-based 2 method. Eigenvector-based 1 method has much larger localization error due to the random initial value of location S.
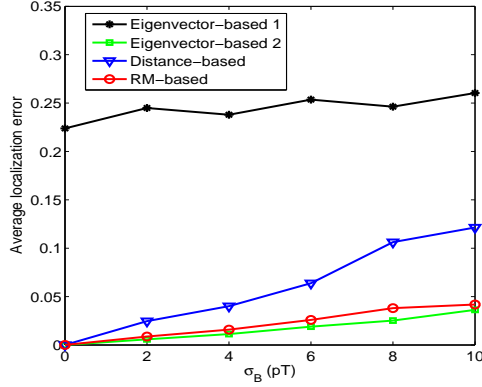
Figure 5. Average localization errors with various σ_B.

Besides the measurement errors of magnetic flux density, there is another factor that also impacts the localization accuracy. We know the three coils in a tri-directional coil structure are mutually orthogonal and the set of three polar angles satisfies equation (8). However, the three coils, in practice, might not be exactly mutual orthogonal. The term *non-orthogonality* is used to describe this situation, as shown in Fig. 6. The solid arrows represent the expected coil axes and the dash arrows represent the actual coil axes, which are deflected by an angle of ζ. The set of three polar angles in the coordinates system against the actual coil axes x′, y′, and z′ does not satisfy (8), causing localization errors. Fig. 7 depicts the localization error with
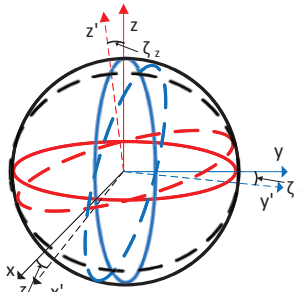
Figure 6. Non-orthogonality of a tri-directional coil.

non-orthogonality, where $\zeta_x = \zeta_y = \zeta_z = 2°$, where $F(\epsilon)$ is the accumulative distribution function (CDF) of the localization error ϵ. We can see the non-orthogonality of a tri-directional coil has significant impact on localization accuracy. RM-based method is more robust against non-orthogonality than Eigenvector-base 2. Distance-based method is the most vulnerable to non-orthogonality. In practice, by careful assembly, non-orthogonality of 2° or smaller can be obtained [27]. For the RM-based method,
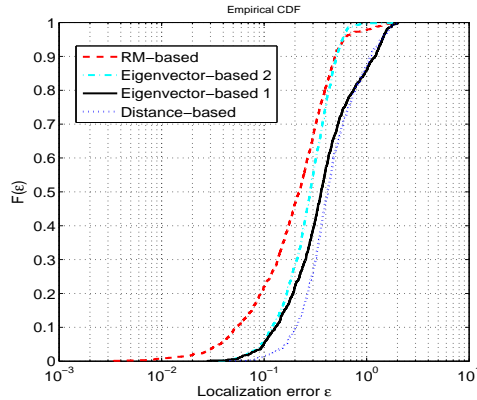
Figure 7. CDF of localization errors with non-orthogonality, $\sigma_B = 0$ pT.

to evaluate the capability solving the localization ambiguity, we set a certain number of anchor nodes that are in the scenario of Fig. 3. The parameter κ denotes the ratio of the anchor nodes that satisfy the special cases in Fig. 3 to the total anchor node number. The average localization errors with various κ is shown in Fig. 8. With increasing percent κ, the average localization errors of Distance-based method increase dramatically while the average localization errors of RM-based method keep almost unchanged. Therefore, RM-based method is capable to solve the localization ambiguity effectively.

4.3. Localization with weights for distance-based method localization. We investigate the relation between transmission distance R and localization error ϵ. We set anchor node A_1 and the sensor node S in space 1 with space size D, and anchor node A_2 in space 2 with space size ρD, where ρ is a scalar that scales
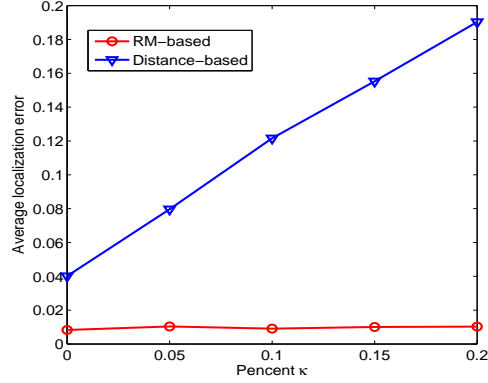
Figure 8. Average localization errors with various percent κ, $\sigma_B = 2$ pT.

up or down space. When ρ is greater than 1, the average transmission distance from anchor node A_2 to the sensor node S is longer than that from anchor node A_1. Notice that no matter what value ρ is, localization errors are still normalized by space size D. To evaluate the influence of transmission distance, we define sub-error $\breve{\epsilon}$ as the Euclidean distance between the sensor node and the chosen location point out of the 8 possible points in a LCS, which is calculated by

$$\breve{\epsilon}_l = ||S - S^*_{ln}|| \tag{40}$$

Fig. 9 depicts the relation between transmission distance, sub-error, and localization error, where $\rho = 2$. We observe that the sub-error $\breve{\epsilon}_2$ from anchor node A_2 is much bigger than sub-error $\breve{\epsilon}_1$ from anchor node A_1, which means the longer transmission distance usually implies larger localization error in the same environment. We also note the localization error ϵ is bigger than $\breve{\epsilon}_1$ and smaller than $\breve{\epsilon}_2$. This observation inspires us that if we consider the reference of anchor node A_2 less and that of anchor node A_1 more, the curve of localization error ϵ will get close to the curve of $\breve{\epsilon}_1$ and far away from $\breve{\epsilon}_2$ curve. Therefore, we add different weight to each anchor node to improve localization accuracy, which is calculated by (38). Placing weights to anchor nodes in
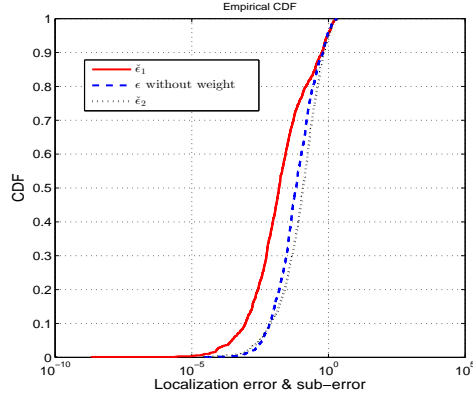
Figure 9. Localization errors and sub-errors without weights, $\rho = 2$, $\sigma_B = 2$ pT.

the localization process, the simulation results are shown in Fig. 10. With weights, the localization error curve is approaching to the curve of $\breve{\epsilon}_1$. In other words, the localization error with weights is reduced significantly compared with the localization error without weights. Since the curve of ϵ with weights is more close to the curve of $\breve{\epsilon}_1$ in Fig. 10, the curve of $\breve{\epsilon}_2$ is much less important in the process of localization. However, we cannot get rid of anchor node A_2 during the localization.
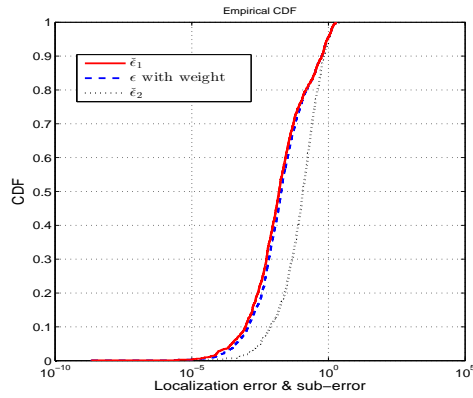
Figure 10. Localization errors and sub-errors with weights, $\rho = 2$, $\sigma_B = 2$ pT.

With increasing scalar ρ, the space where anchor node A_2 is located becomes bigger and the average transmission distance from anchor node A_2 to the sensor node is getting longer. Although it is possible, in practice, we are incapable of measuring the magnetic flux density when the transmission distance is too long, we don't consider this situation in our simulations as long as it is still in the near-field range. We just present the relation of the transmission distance and the localization error.

Fig. 11 demonstrates the average localization error with increasing scalar ρ. With bigger scalar ρ, the localization error without weights is larger than that with weights. Therefore, we conclude that the localization scheme with weights is especially effective in the situation where the sensor node is close to one anchor node and far away from another anchor node.
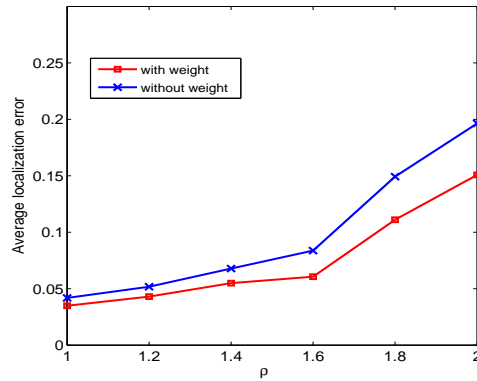
Figure 11. Average localization errors with and without weights.

5. CONCLUSION

In this paper, we propose two MI-based localization methods which can be applied in some challenging environments, such as underground, underwater, inside of animals, and indoor. These methods are able to locate sensor nodes with arbitrary orientations and positions in 3-D, only assisted with two anchor nodes. Numerous simulations are done to verify these two methods and evaluate their performances.

The RM-based method can reach high localization accuracy with measurement errors or noise considered. The Distance-based method has less computational complexity and is faster but may encounter localization ambiguity in some cases. The RM-based method can be utilized in these cases since it is able to solve the localization ambiguity. Therefore, these two localization methods can be applied to different applications according to the system requirements. In addition, we derived a closed-form formula of transmission distance. Simulation results show our distance estimation has higher accuracy comparing with the wide-used RSSI model.

REFERENCES

[1] I. F. Akyildiz, P. Wang, and Z. Sun, "Realizing underwater communication through magnetic induction," *IEEE Communications Magazine*, vol. 53, no. 11, pp. 42–48, 2015.

[2] H. P. Tan, R. Diamant, W. K. Seah, and M. Waldmeyer, "A survey of techniques and challenges in underwater localization," *Ocean Engineering*, vol. 38, no. 14, pp. 1663–1676, 2011.

[3] I. F. Akyildiz and E. P. Stuntebeck, "Wireless underground sensor networks: Research challenges," *Ad Hoc Networks*, vol. 4, no. 6, pp. 669–686, 2006.

[4] B. Gozick, K. P. Subbu, R. Dantu, and T. Maeshiro, "Magnetic maps for indoor navigation," *IEEE Transactions on Instrumentation and Measurement*, vol. 60, no. 12, pp. 3883–3891, 2011.

[5] J. Haverinen and A. Kemppainen, "Global indoor self-localization based on the ambient magnetic field," *Elsevier Robotics and Autonomous Systems*, vol. 57, no. 10, pp. 1028–1035, 2009.

[6] D. Navarro and B. Gines, "Magnetic map building for mobile robot localization purpose," in *IEEE Conference on Emerging Technologies Factory Automation*, 2009, pp. 1–4.

[7] A. Markham, N. Trigoni, D. W. Macdonald, and S. A. Ellwood, "Underground localization in 3-D using magneto-inductive tracking," *IEEE Sensors Journal*, vol. 12, no. 6, pp. 1809–1816, 2012.

[8] S. A. Rahok and O. Koichi, "Odometry correction with localization based on landmarkless magnetic map for navigation system of indoor mobile robot," in *4th International Conference Autonomous Robots and Agents, 2009. ICARA 2009.*, pp. 572–577.

[9] C. P. Davis, W. C. Chew, W. W. Tucker, and P. R. Atkins, "A null-field method for estimating underground position," *IEEE Transactions on Geoscience and Remote Sensing*, vol. 46, no. 11, pp. 3731–3738, 2008.

[10] S. Hashi, M. Toyoda, S. Yabukami, K. Ishiyama, Y. Okazaki, and K. I. Arai, "Wireless magnetic motion capture system-compensatory tracking of positional error caused by mutual inductance," *IEEE Transactions on Magnetics*, vol. 46, no. 6, pp. 2364–2366, 2007.

[11] S. Hashi, M. Toyoda, M. Ohya, Y. Okazaki, S. Yabukami, K. Ishiyama, and K. I. Arai, "Magnetic motion capture system using LC resonant magnetic marker composed of Ni-Zn ferrite core," *Journal of applied physics*, vol. 99, no. 8, 2006.

[12] E. P. A. Plotkin, "3-D magnetic tracking of a single subminiature coil with a large 2-D array of uniaxial transmitters," *Transactions on Magnetics*, vol. 39, no. 5, pp. 3295–3297, 2003.

[13] G. Placidi, D. Franchi, A. Maurizi, and A. Sotgiu, "Review on patents about magnetic localisation systems for in vivo catheterizations," *Recent Patents on Biomedical Engineering*, vol. 2, no. 1, pp. 58–64, 2009.

[14] A. M. Franz, T. Haidegger, W. Birkfellner, K. Cleary, T. M. Peters, and L. Maier-Hein, "Electromagnetic tracking in medicine-a review of technology, validation, and applications," *IEEE transactions on medical imaging*, vol. 33, no. 8, pp. 1702–1725, 2014.

[15] H. Huang, Y. R. Zheng, and W. M. Duan, "Pseudo-noise based time of arrival estimation for underwater acoustic sensor localization," in *OCEANS 2016-Shanghai.* IEEE, 2016, pp. 1–5.

[16] Z. Zhou, J.-H. Cui, and S. Zhou, "Efficient localization for large-scale underwater sensor networks," *Ad Hoc Networks*, vol. 8, no. 3, pp. 267–279, 2010.

[17] J. Albowicz, A. Chen, and L. Zhang, "Recursive position estimation in sensor networks," in *Ninth International Conference on Network Protocols, 2001.* IEEE, 2001, pp. 35–41.

[18] M. C. Vuran and I. F. Akyildiz, "Channel model and analysis for wireless underground sensor networks in soil medium," *Physical Communication*, vol. 3, no. 4, pp. 245–254, 2010.

[19] L. E. Emokpae, S. DiBenedetto, B. Potteiger, and M. Younis, "Ureal: underwater reflection-enabled acoustic-based localization," *IEEE Sensors Journal*, vol. 14, no. 11, pp. 3915–3925, 2014.

[20] L. E. Emokpae and M. Younis, "Throughput analysis for shallow water communication utilizing directional antennas," *IEEE Journal on Selected Areas in Communications*, vol. 30, no. 5, pp. 1006–1018, 2012.

[21] R. J. Blakely, *Potential Theory in Gravity and Magnetic Applications.* Cambridge, U.K: Cambridge Univ, 2001.

[22] M. A. Nixon, B. C. McCallum, W. R. Fright, and N. B. Price, "The effects of metals and interfering fields on electromagnetic trackers," *Presence*, vol. 7, no. 2, pp. 204–218, 1998.

[23] V. F. Labson, A. Becker, H. F. Morrison, and U. Conti, "Geophysical exploration with audiofrequency natural magnetic fields," *Geophysics*, vol. 50, no. 4, pp. 656–664, 1985.

[24] F. H. Raab, "Noise model for low-frequency through-the-earth communication," *Radio Sci*, vol. 45, no. 6, pp. 1–7, 2010.

[25] A. Sheinker, B. Ginzburg, N. Salomonski, L. Frumkis, and B. Z. Kaplan, "Localization in 2D using beacons of low frequency magnetic field," *IEEE Journal of Selected Topics in Applied Earth Observations and Remote Sensing*, vol. 6, no. 2, pp. 1020–1030, 2013.

[26] X. Tan, Z. Sun, and P. Wang, "On localization for magnetic induction-based wireless sensor networks in pipeline environments," in *2015 IEEE International Conference on Communications (ICC).* IEEE, 2015, pp. 2780–2785.

[27] A. Sheinker, B. Ginzburg, N. Salomonski, L. Frumkis, and B. Z. Kaplan, "Localization in 3-D using beacons of low frequency magnetic field," *IEEE transactions on instrumentation and measurement*, vol. 62, no. 12, pp. 3194–3201, 2013.

[28] E. Slottke and A. Wittneben, "Accurate localization of passive sensors using multiple impedance measurements," in *Vehicular Technology Conference (VTC Spring), 2014 IEEE 79th.* IEEE, 2014, pp. 1–5.

[29] A. Radchenko, D. Pommerenke, G. Chen, P. Maheshwari, S. Shinde, V. Pilla, and Y. R. Zheng, "Real time bridge scour monitoring with magneto-inductive field coupling," in *SPIE Smart Structures and Materials+ Nondestructive Evaluation and Health Monitoring.* International Society for Optics and Photonics, 2013, pp. 86 922A–86 922A.

[30] F. H. Raab, E. B. Blood, T. O. Steiner, and H. R. Jones, "Magnetic position and orientation tracking system," *IEEE Transactions on Aerospace and Electronic systems*, no. 5, pp. 709–718, 1979.

[31] S. Boyd and L. Vandenberghe, *Convex Optimization.* Cambridge, U.K.: Cambridge Univ. Press, 2004.

[32] T. E. Abrudan, Z. Xiao, A. Markham, and N. Trigoni, "Underground incrementally deployed magneto-inductive 3-d positioning network," *IEEE Transactions on Geoscience and Remote Sensing*, vol. 54, no. 8, pp. 4376–4391, 2016.

[33] T. E. Abrudan, O. Kypris, N. Trigoni, and A. Markham, "Impact of rocks and minerals on underground magneto-inductive communication and localization," *IEEE Access*, vol. 4, pp. 3999–4010, 2016.

[34] Y. Zhang, S. Xing, Y. Zhu, F. Yan, and L. Shen, "Rss-based localization in wsns using gaussian mixture model via semidefinite relaxation," *IEEE Communications Letters*, 2017.

II. NODE LOCALIZATION WITH AOA ASSISTANCE IN MULTI-HOP UNDERWATER SENSOR NETWORKS

Huai Huang and Yahong Rosa Zheng

Department of Electrical & Computer Engineering

Missouri University of Science and Technology

Rolla, Missouri 65409–0050

Email: {hh6v8, zhengyr}@mst.edu

ABSTRACT

This paper proposes a novel node localization method for underwater wireless networks (UWSNs) in 2-D and 3-D spaces, respectively, where only a small number of anchor nodes are available. Our scheme estimates distances from anchor nodes to sensor nodes via multi-hops with the help of angle of arrival (AoA) measurements. By forwarding distances hop-by-hop through the wireless network, the distance estimations can be flooded to the whole network even if the network is sparse. Once a sensor node has its distance estimates to at least three (in 2-D) or four (3-D) anchor nodes, it can compute its own location. In contrast to existing multi-hop methods, such as DV-hop, DV-distance, Euclidean method, Cosine-law method, and Distance-based method, our proposed method uses rotation matrices between neighboring nodes to estimate distances to anchor nodes, with higher accuracy. Therefore, the proposed method can improve localization accuracy significantly. In addition, we derived the formulas of weights added to anchor nodes to improve localization accuracy according to AoA measurement errors and the number of hops. Simulation results show that our proposed method outperforms the existing multi-hop localization schemes

in terms of localization accuracy and distance estimation. The concept of weights on anchor nodes improves localization accuracy remarkably when AoA measurement errors are relatively large.

1. INTRODUCTION

Underwate sensor networks (UWSNs) have found important applications in ocean exploration, critical structure monitoring, coastal surveillance, motion tracking, and disaster mitigation [1]. For example, the melting process of the polar ice sheets, which contributes to the sea level rises, calls for an underwater Ad-Hoc network to provide the timely sea level monitoring. UWSNs include a large number of randomly placed wireless nodes with sensors [2, 3]. These nodes are used to collect hydrologic data such as pressure, salinity, and temperature.

In many applications of UWSNs, the position knowledge of wireless sensor nodes is desirable otherwise the sensing information collected is meaningless. Therefore, localization is a must-do task in UWSN applications [4].

The typical UWSN scenario depicted in Fig. 1 has only a small number of nodes with location-awareness from GPS or surface buoys. This type of nodes is named *anchor* nodes. Another type of nodes in a UWSN are equipped with sensors to collect useful data in water, and are called *sensor* nodes. Sensor nodes cannot communicate directly with GPS or buoys, thus have to estimate their own locations by communicating with anchor nodes around them. The accuracy and coverage of localizations in an UWSN are the main concerns, especially in a large-scale sparse network where the number of anchor nodes is a small fraction of the total number of nodes and the node degree is small. The Global Positioning System (GPS) wide-used in terresterial sensor networks is not feasible underwater because the radio-frequency signals utilized by GPS have very limited communication range due to
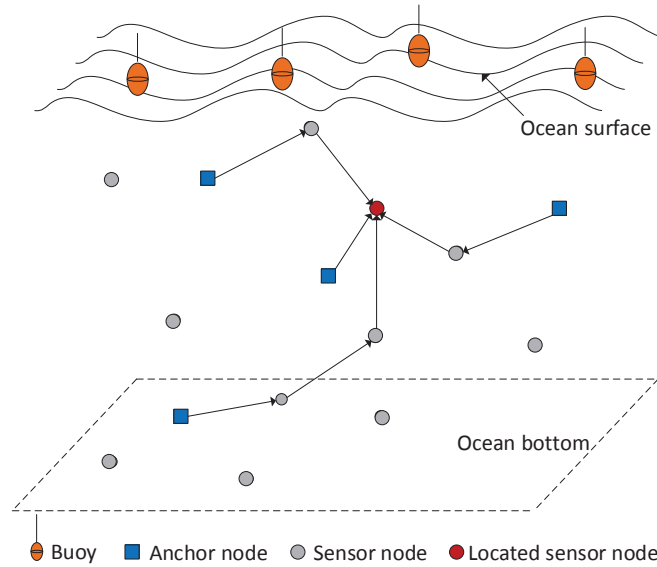
Figure 1. The framework of underwater sensor networks with multi-hop propagation.

the strong propagation loss in water[5]. Therefore, acoustic signals, optical signals, and Magnetic-Induction (MI) signals are employed in underwater communication and localization [6].

The existing localization schemes in underwater wireless sensor networks are usually classified into two categories: range-based schemes and range-free schemes [7, 8]. Since range-free schemes can only obtain coarse localization, range-based schemes are widely used. Range-based schemes consist of three phases: distance estimation, position estimation, and refinement. The distances to anchor nodes are measured by several schemes: received signal strength indicator (RSSI), time difference of arrival (TDoA), and time of arrival (ToA) [4]. Most range-based localization schemes in UWSNs use ToA or TDoA thanks to the slow sound propagation in water (about 1500 m/s), which can achieve better accuracy than the RSSI schemes [7]. Due to the limited communication range of acoustic signals underwater, only nodes within a certain range can communicate directly with each other to get range or angle estimations. The nodes within a communication range are called neighbors.

The traditional localization schemes require distance estimates to at least three (in 2-D space) or four (in 3-D space) anchor nodes to calculate the sensor node's location by the trilateration method. However, in a large-scale sparse wireless network, due to sensor nodes moving and diffusing after deployed, there are some isolated nodes that cannot reach enough anchor nodes and thus are incapable of self-localization [9]. It is not feasible to have the beacons emit with large power to cover the whole network due to the high power usage and communication collisions[10]. Some schemes have been developed to do localization in this case. AUV-aided algorithms use traveling AUV to assist isolated nodes localization[11]. In a relatively dense network, the recursive localization method reaches high localization coverage [12]. However, when the network is sparse, the localization coverage is significantly reduced because the recursive localization method requires at least four nodes (in 3-D space) with position-awareness around the to-locate sensor node. To extend the localization coverage in a sparse network, several localization schemes have been proposed, utilizing multi-hop distance propagations: DV-hop, DV-distance, and Euclidean method [10]. These schemes forward distances via intermediate nodes hop by hop to obtain distance estimates to anchor nodes. Once a sensor node obtains at least four anchor nodes distance estimations, trilateration algorithm is employed to do localization. The DV-hop and DV-distance methods can only achieve coarse localization and are sensitive to anisotropic topologies. The Euclidean method can achieve higher localization accuracy but much lower localization coverage than the DV-hop and DV-distance methods. In recent years, to improve localization accuracy, some other algorithms based on multi-hop propagation have been proposed. Paper [13] uses the law of cosine to estimate distances from anchor nodes to isolated nodes. We call this method as the Cosine-law method. The Cosine-law method has higher localization accuracy,

but can be applied only in 2-D space. Paper [14] employs greedy algorithm to find the shortest path as the distance estimation, which is called as the Distance-based method in this paper.

In this paper, we aim to improve localization accuracy and keep high localization coverage in a large-scale sparse underwater wireless sensor network based on multi-hop propagation. Our proposed scheme takes advantage of angle measurements of incoming signals which are called angle of arrival (AoA) measurements to locate sensor nodes in 2-D and 3-D spaces, respectively. Recent works in the field [15] have shown the feasibility of utilizing AoA measurements in underwater networks. The paper [16] utilizes AoA measurements to provide the 3-D ranging estimation in an underwater environment. Papers [17, 18] show localization in underwater sensor networks based on AoA measurements. The AoA capability is usually achieved by using directional antennas [19] or antenna array. In this paper, we assume each node in UWSNs has the capability of measuring the AoA from its neighbors. The simulation results show that our proposed scheme achieves higher localization and distance accuracy than the existing multi-hop localization schemes, with almost the same high localization coverage as the DV-hop and DV-distance methods.

2. RELATED WORK

Several existing multi-hop localization methods are introduced in this section.

2.1. DV-hop. The DV-hop scheme counts distances between nodes in hops [10]. Each node in a network has a hop table and exchange the table with its neighbors. The hop forwarding starts from an anchor node and floods into the sensor network. When a node receives the hop table from its neighbor, the node updates its own hop table. Once the hop-forwarding hits another anchor node, it estimates the average size of one hop based on the absolute locations of the two anchor nodes. A sensor node computes the distance in meters to the anchor node by the calculated

average hop size and the hop table. We can see that DV-hop method is simple and immune to distance measurement errors. However, it can only provide coarse distance and localization estimations.

2.2. DV-distance. The DV-distance approach is similar to the DV-hop method in terms of the forwarding procedure [10]. The difference lies in that the forwarded distance between nodes is in *meters*, rather than in *hops*. The distance from an anchor node to a sensor node is then calculated by accumulating distances hop by hop. The DV-distance scheme is still coarse because the real distance between a sensor node and an anchor node is the distance of the line-of-sight, not the cumulative hop-by-hop distance. In addition, both the DV-hop and DV-distance methods are sensitive to the topology of a network and can be applied in 2-D and 3-D spaces.

2.3. Euclidean method. The Euclidean method calculates the *Euclidean* distances from sensor nodes to anchor nodes [10]. Therefore, this method provides more accurate distance estimation. However, this method requires more neighbors around a sensor node with distance estimates to an anchor node. This requirement restricts the localization coverage. The Euclidean method can do localization in 2-D space.

2.4. Cosine-law method. Paper [13] proposes a multi-hop distance estimation method based on the law of cosines. It assumes each node in a wireless network is able to measure distances and angles of incoming signals from its neighboring nodes. Then, the law of cosines is employed to calculate distances and angles for nodes with more hops to an anchor node. This method can calculate the Euclidean distances to anchor nodes and improve localization accuracy. However, the Cosine-law method is sensitive to measurement errors and only feasible in 2-D space.

2.5. Distance-based localization. Paper [14] employs intermediate nodes as routers between an anchor node and a sensor node to find the shortest distance between them by the greedy algorithm. It assumes the measured distance in all

radio runtime based measurement systems is too long and not too short because of reflections and multipath effects [14]. This method has better localization accuracy than DV-distance due to the shorter path search and can be used in 2-D and 3-D localizations.

3. THE PROPOSED SCHEMES

3.1. AoA theory. Each node in a network has axes against which the arrival angles of incoming signals from neighbors are reported, as shown in Fig. 2. The axes in each node form a local coordinate system (LCS). After deployment, the axes of a node or the LCS has an arbitrary direction, which is represented by the bold arrow in Fig. 2. The term *bearing* represents the angle measured with respect to a neighbor. In this paper, bearings at each node with respect to its neighbors provides AoA measurements. For example, at node N_2 in the 2-D space of Fig. 2(a), the bearing against the axis at node N_2 provides the AoA measurements of θ_{12} and θ_{32} from two neighbors N_1 and N_3, respectively. In 3-D space, the AoA measurement includes elevation and azimuth angles. In the example of Fig. 2(b), the AoA measurement at node N_2 from node N_1 is θ_{12} and β_{12}.

(a) 2-D   (b) 3-D
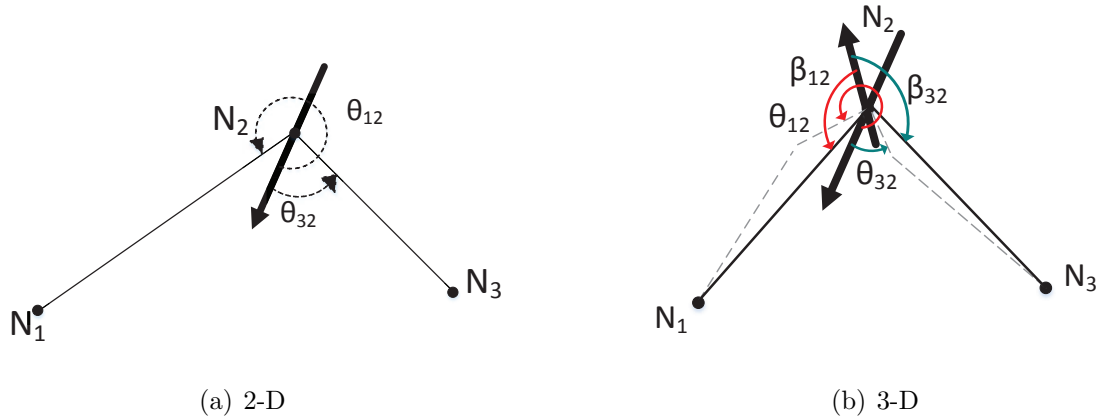
Figure 2. AoA measurements at a node.

3.2. The proposed localization algorithm. In this section, we propose a node localization method with multi-hop propagation by taking advantage of AoA measurements. Our proposed localization method can be applied in both 2-D and 3-D spaces, with higher accuracy.

A simple scenario of UWSNs is depicted in Fig. 3, where circles denote sensor nodes, the rectangle denotes an anchor node, and the number in each circle and rectangle denotes the hops from the anchor node. Fig. 3 refers to one anchor node only, since the multi-hop propagation behaves identically and independently for all anchor nodes in a UWSN. The node set including all anchor nodes and sensor nodes in a network is expressed as $\mathbf{N}=\{N_1,N_2,...,N_N\}$. In this example, sensor nodes N_2, N_3, and N_4 have 1 hop, nodes N_5, N_6 and N_8 have 2 hops, node N_7 has 3 hops from the anchor node N_1, and the anchor node has 0 hop. The sensor nodes are divided into three types according to the number of hops from the anchor node.

Figure 3. A network with multi-hop propagation.

1) one-hop nodes: Anchor nodes broadcast a message that includes their ID, coordinates and transmitting time stamp to the neighboring sensor nodes. The sensor nodes that receive this message can measure the AoA, and the distance from the anchor node. Therefore, the coordinates of the anchor node in the LCS of a one-hop sensor node are available.

2) two-hop nodes: All nodes can communicate directly with their neighboring nodes and measure distances and AoAs between one another. Therefore, the locations of two-hop nodes in the LCSs of o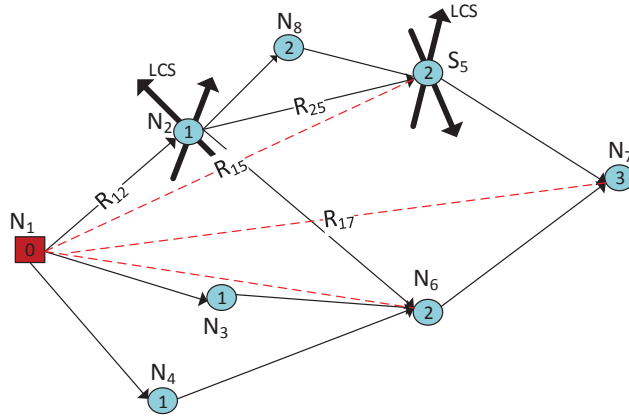ne-hop nodes are available. Since locations of anchor nodes in the LCSs of one-hop nodes are also available, the distances of nodes with 2 hops to anchor nodes can be estimated.

3) greater-than-two-hop nodes: They can not estimate the distances to an anchor node like one-hop or two-hop nodes because they are not neighboring with the anchor node nor with one-hop nodes. Nodes between an anchor node and a greater-than-two-hop node are used as intermediate routers and the rotation matrix between two routers is employed to forward coordinates and distances hop by hop. The intermediate nodes not only send their own node ID to nodes with more hops, but also the ID, coordinates of anchor nodes.

Once receiving a message from a neighbor, a sensor node which is considered as the current node, updates its hops and builds an entry of the information table shown in Fig. 4 through some computations. We assume the current sensor node is N_j and it is receiving signals from its neighboring node N_i. The first seven terms in the table refer to the neighboring node N_i that might not be an anchor node, which include: (1) ID1: the neighboring node's identifier from the incoming signal;(2) AoA: angle of arrival from the neighboring node with ID1; (3)ToA: time of arrival from the neighboring node with ID1; (4) Hop: the hop number of the neighboring node N_i pluses one; (5) Coordinate1: once ToA and AoA from the neighboring node are obtained, the coordinates of the neighboring node N_i in the LCS of the current

node N_j are calculated as $\mathbf{c}_{ij}$ which is sent back to the neighboring node N_i; (6) Coordinate2: similarly, the coordinate $\mathbf{c}_{ji}$ is the coordinates of the current node N_j in the LCS of the neighboring node N_i and sent by node N_i; (7) Coordinate3: the coordinates of the anchor node that node N_i has coordinates estimate to in the LCS of node N_i. The last two terms in the table refer to the anchor node, which include: (8) ID2: the anchor node's ID; (9) Coordinate4: the absolute coordinates of the anchor node. If the neighboring node is an anchor node, ID1 and ID2 are identical and Coordinate3 is null. If the neighboring node N_i has no coordinates estimation of an anchor node, the terms of Coordinate3, ID2, and Coordinate4 are null.

ID1	AoA	ToA	Hop	Coordinates1	Coordinates2	Coordinates3	ID2	Coordinates4

Figure 4. Information table structure.

The first step of the proposed localization method is to estimate distances of the current node to an anchor node. Since one-hop nodes can directly communicate with anchor nodes, the distances between these sensor nodes and anchor nodes, such as distance R_{12} in Fig. 3, are measurable. However, the distances of nodes with more than 2 hops to an anchor node, like distances R_{15} and R_{17} cannot be obtained by direct communications.

All nodes, equipped with multi-modal directional piezoelectric underwater transducers, are capable of measuring both azimuth and elevation angles [16]. The AoA measurement at a sensor node N_j of the incoming signal form a neighboring sensor node N_i is denoted as $\{\theta_{ij}, \beta_{ij}\}$, where β_{ij} is the elevation angle, and θ_{ij} is the azimuth angle.

According to the transformation of Spherical Coordinate System (SCS) (3-D) to Cartesian Coordinate System (CCS) (3-D), the coordinates of node N_i in the LCS of node N_j are defined as

$$\mathbf{c}_{ij} = [x_{ij}, y_{ij}, z_{ij}]^T \tag{1}$$

where $[]^T$ represents transpose of a matrix and x_{ij}, y_{ij} and z_{ij} are calculated by

$$x_{ij} = R_{ij} \cos \beta_{ij} \cos \theta_{ij}$$

$$y_{ij} = R_{ij} \cos \beta_{ij} \sin \theta_{ij} \qquad (2)$$

$$z_{ij} = R_{ij} \sin \beta_{ij}$$

where R_{ij} is the distance from node N_i to node N_j. Once the coordinates of two nodes N_i and $N_{i'}$ in the LCS of node N_j are obtained, the distance $R_{ii'}$ between nodes N_i and $N_{i'}$ is calculated by

$$R_{ii'} = \|\mathbf{c}_{ij} - \mathbf{c}_{i'j}\| \qquad i \neq i' \qquad (3)$$

where $\| \cdot \|$ denotes the vector norm 2. If node $N_{i'}$ is an anchor node and node N_j is one-hop, the distance estimation of two-hop node N_i to the anchor node is available by (3). For example, in the scenario of Fig. 3, the two-hop node N_5 estimates its distance to the anchor node N_1 via the one-hop node N_2 as an intermediate router.

In a large-scale network, to improve localization coverage, it is desirable to obtain distance estimations of nodes with more than 2 hops to an anchor node. However, Eq (3) is only applied to two-hop nodes. In this section, we propose an algorithm that estimates distances of greater-than-two-hop nodes to anchor nodes, such as distance R_{17} in Fig. 3. Since node N_7 is a neighbor of node N_5, the distance R_{17} can be computed by (3) if the coordinates of anchor node N_1 in the LCS of node N_5 is available, i.e., the term of Coordinate3 in the information table of node N_7 is the key point. In the example of Fig. 3, for node N_7, the term of Coordinate1 is $\mathbf{c}_{57}$, the term of Coordinate2 is $\mathbf{c}_{75}$, and the term of Coordinate3 is $\mathbf{c}_{15}$. We know the coordinates of node N_1 in the LCS of node N_2 is computable since node N_2 only has 1 hop, and the coordinates of node N_2 in the LCS of node N_5 is computable since node N_2 is a neighbor of node N_5. If we can find the rotation matrix between the

two LCSs of nodes N_2 and N_5, the the coordinates of anchor node N_1 in the LCS of node N_5 is available. Therefore, the key point is to find the rotation matrix between two neighboring LCSs.

Assume nodes N_i and N_j are neighbors, and we want to figure out the rotation matrix $\mathbf{Q}_{ij}$ between their LCSs. If the two nodes have at least one common neighbor N_k additionally, which means node N_k can communicate directly with both nodes N_i and N_j, then the rotation matrix $\mathbf{Q}_{ij}$ satisfies the following equations

$$
\begin{cases}
\mathbf{Q}_{ij}\mathbf{c}_{ji} = -\mathbf{c}_{ij} \\
\mathbf{Q}_{ij}\mathbf{c}_{ki} = \mathbf{c}_{kj} - \mathbf{c}_{ij} \\
\mathbf{Q}_{ij}^{T} * \mathbf{Q}_{ij} = \mathbf{I}
\end{cases}
\tag{4}
$$

where $\mathbf{I}$ is a identity matrix of size 3×3, and the third equation in (4) is the property a rotation matrix must satisfy. Note that it is possible there are several common neighboring nodes between nodes N_i and N_j after the deployment, then k has multiple values which results in multiple equations with the same similar expression of the second equation in (4). We define two matrices $\mathbf{X}$ and $\mathbf{Y}$ of size $3 \times (M + 1)$, where M is the number of common neighboring nodes between nodes N_i and N_j. Matrix $\mathbf{X} = [\mathbf{c}_{ji}, \mathbf{c}_{ki}]$, and matrix $\mathbf{Y} = [-\mathbf{c}_{ij}, \mathbf{c}_{kj} - \mathbf{c}_{ij}]$. Therefore, the more general expression of (4) is

$$
\begin{cases}
\mathbf{Q}_{ij}\mathbf{X} = \mathbf{Y} \\
\mathbf{Q}_{ij}^{T}\mathbf{Q}_{ij} = \mathbf{I}
\end{cases}
\tag{5}
$$

Without noise or measurement errors considered, $K = 1$ is enough to solve (5) in 3-D space, i.e. at least one common neighbor between nodes N_i and N_j is required to calculate the matrix $\mathbf{Q}_{ij}$. When noise or measurement errors are considered, more common neighbor nodes result in the better estimation of the matrix $\mathbf{Q}_{ij}$. We use

the method in [20] to solve matrix $\mathbf{Q}_{ij}$ in (5). We optimize

$$\arg\min_{\mathbf{Q}_{ij}} \sum_{m=1}^{M+1} \|\mathbf{Q}_{ij}\mathbf{X}_m - \mathbf{Y}_m\|^2 \tag{6}$$

where $\mathbf{X}_m$ is the mth column of the matrix $\mathbf{X}$, and $\mathbf{Y}_m$ is the mth column of the matrix $\mathbf{Y}$. We define a matrix $\mathbf{S}$ of size 3×3 and $\mathbf{S} = \mathbf{X}\mathbf{Y}^T$. Matrix $\mathbf{S}$ is decomposed by singular value decomposition (SVD) as

$$\mathbf{S} = \mathbf{U}\boldsymbol{\Sigma}\mathbf{V}^T \tag{7}$$

where $\boldsymbol{\Sigma}$ is a diagonal matrix with singular values on diagonal entries, matrices $\mathbf{U}$ and $\mathbf{V}$ are unitary matrices, with left-singular vectors and right-singular vectors of matrix $\mathbf{S}$ as columns, respectively. According to [20], the rotation matrix $\mathbf{Q}_{ij}$ is calculate by

$$\mathbf{Q}_{ij} = \mathbf{V} \begin{bmatrix} 1 & 0 & 0 \\ 0 & 1 & 0 \\ 0 & 0 & \det(\mathbf{V}\mathbf{U}^T) \end{bmatrix} \mathbf{U}^T \tag{8}$$

The diagonal matrix in (8) includes the $\det(\mathbf{V}\mathbf{U}^T)$ to guarantee the calculated matrix $\mathbf{Q}_{ij}$ is a rotation instead of a reflection [20].

Once the matrix $\mathbf{Q}_{ij}$ is obtained, the coordinates of the anchor node $N_{i'}$ in node N_j is calculable by

$$\mathbf{c}_{i'j} = \mathbf{Q}_{ij}\mathbf{c}_{i'i} + \mathbf{c}_{ij} \tag{9}$$

where $\mathbf{c}_{ij}$ is considered as the original point offset and we assume the coordinates $\mathbf{c}_{i'i}$ is known. For example, in Fig. 3, the coordinates of anchor node N_1 in LCS of node N_5 are calculated by $\mathbf{c}_{15} = \mathbf{Q}_{25}\mathbf{c}_{12} + \mathbf{c}_{25}$, and the matrix $\mathbf{Q}_{25}$ is calculated by (8). Therefore, the coordinates of an anchor node at the LCS of an two-hop node is available. The distance $R_{i'i''}$ of node $N_{i''}$ that has 3 hops from the anchor node $N_{i'}$

and is also a neighbor of node N_j is computed by

$$R_{i'i''} = \|\mathbf{c}_{i'j} - \mathbf{c}_{i''j}\| \tag{10}$$

For example, in Fig. 3, the distance R_{17} with 3 hops is computed by $R_{17} = \|\mathbf{c}_{15} - \mathbf{c}_{75}\|$, where $j = 5$, $i' = 1$, and $i'' = 7$. By the same way, the distance estimation can be flooded into nodes with more than 3 hops.

In a network, the distance of a sensor node to an anchor node might be estimated via different intermediate node routers to form different routes. For example, for node N_7, one route is $N_1 \rightarrow N_2 \rightarrow N_5 \rightarrow N_7$ and another route is $N_1 \rightarrow N_3 \rightarrow N_6 \rightarrow N_7$. Both of the routes have 3 hops. In Fig. 3, there is another route for node N_7: $N_1 \rightarrow N_2 \rightarrow N_8 \rightarrow N_5 \rightarrow N_7$. However, this route has one more hop than the other two routes. Due to measurement errors and noise, each hop unavoidable brings estimation errors. Hence, we want to keep a route as fewer hops as possible. Then the routes with more hops are discarded. Considering noise and measurement errors, multiple routes with different intermediate nodes generate different intermediate rotation matrices and coordinate estimations. For example, in Fig. 3, we have different $\mathbf{c}_{16}$ estimations via routes $N_1 \rightarrow N_3 \rightarrow N_6$ and $N_1 \rightarrow N_4 \rightarrow N_6$. Our proposed method averages all coordinate estimations from multiple routes at each sensor node to reduce the impact of the noise and measurement errors.

Additionally, for each sensor node, different routes also generate different distance estimations to anchor nodes with noise considered. We average all distance estimations at each sensor node to get the final distance estimation.

This method is also feasible in 2-D space, and the AoA only has one angle measurement shown in Fig2. the coordinates of node N_i in the LCS of node N_j are defined as

$$\mathbf{c}_{ij} = [x_{ij}, y_{ij}]^T \tag{11}$$

where x_{ij}, y_{ij} are calculated as

$$x_{ij} = R_{ij} \cos \theta_{ij}$$
$$y_{ij} = R_{ij} \sin \theta_{ij}$$

(12)

One thing we should point out is that common neighboring nodes are not prerequisite to calculate the rotation matrix between two LCSs in 2-D space, although at least one common neighboring node is required in 3-D space. In other words, the rotation matrix can be completely determined without the second equation in (5) when noise or measurement errors are not considered. This property results higher localization coverage in 2-D space than in 3-D space.

3.3. Weighted least squares. Once a sensor node obtains distances to at least four (in 3-D) or three (in 2-D) anchor nodes, its position can be computed by trilateration algorithm, like the located sensor node in Fig 1. Least Squares (LS) method is usually used to estimate the location with more anchor nodes available [21]. Let (X_t, Y_t, Z_t) be the coordinates of the tth anchor node in the global coordinate system (GCS) for $t = 1, \cdots, n$. The coordinates and the estimated distance (R_t) from the tth anchor satisfy the following set of equations:

$$\begin{bmatrix} (X_1 - X)^2 + (Y_1 - Y)^2 + (Z_1 - Z)^2 \\ \vdots \\ (X_n - X)^2 + (Y_n - Y)^2 + (Z_n - Z)^2 \end{bmatrix} = \begin{bmatrix} R_1^2 \\ \vdots \\ R_n^2 \end{bmatrix}$$

(13)

where (X, Y, Z) is the coordinates of the to-locate sensor node in the GCS. By subtracting the nth equation from each other equation in (13), a general matrix form is written by

$$\mathbf{HC} = \mathbf{B}$$

(14)

where

$$\mathbf{H} = 2 \begin{bmatrix} X_1 - X_n & Y_1 - Y_n & Z_1 - Z_n \\ \vdots & \ddots & \vdots \\ X_{n-1} - X_n & Y_{n-1} - Y_n & Z_{n-1} - Z_n \end{bmatrix} \qquad (15)$$

$$\mathbf{C} = \begin{bmatrix} X & Y & Z \end{bmatrix}^T \qquad (16)$$

$$\mathbf{B} = \begin{bmatrix} X_1^2 - X_n^2 + Y_1^2 - Y_n^2 + R_n^2 - R_1^2 \\ \vdots \\ X_{n-1}^2 - X_n^2 + Y_{n-1}^2 - Y_n^2 + R_n^2 - R_{n-1}^2 \end{bmatrix} \qquad (17)$$

In this paper, we employ the weighted LS to improve localization accuracy, i.e., we assign a weight to each anchor node to indicate how significant the anchor node is during the localization. In a network, a sensor node might have different numbers of hops to its available anchor nodes, which is called as *mix-hop* as shown in Fig6, where the dash lines denote routes with multi-hop via intermediate nodes. Since each hop unavoidably brings some errors due to measurement means, noise [22], and rotation matrix estimations, it is reasonable to assume that more hops cause more errors. Therefore, we choose routes with as fewer hops as possible and assign weights as a function of the number of hops that a sensor node has from an anchor node. Besides the number of hops, other factors also impact the weights, such as communication range, measurement errors. Since the estimated localization error is a complicated nonlinear function of the number of hops and other factors, we do numerous simulations and use regression analysis to find the functions that fit the numerical simulated results. Our extensive simulations found that the localization errors are related to many factors: communication range, distance measurement errors, AoA measurement errors, and the number of hops. For the sake of simplicity, we consider only two major factors that affect most: AoA measurement errors and the number of hops, which

Table 1. Lookup table for parameters a, b and c

	2-D			3-D		
	a	b	c	a	b	c
$\sigma_A : [0°, 2.5°)$	0.946	0.991	1.873	2.588	0.578	0.738
$\sigma_A : [2.5°, 7.5°)$	1.132	1.361	1.926	1.981	1.171	1.315
$\sigma_A : [7.5°, 12.5°)$	2.240	1.395	0.331	9.1	1.107	-6.487
$\sigma_A : [12.5°, 17.5°)$	3.454	3.107	1.620	-0.750	1.203	-11.04

can give us a rough formula of weights. We define a parameter ρ as

$$\rho = \frac{\sum\limits_{l \in L} \|\hat{\mathbf{C}}_l - \mathbf{C}_l\|^2}{L} \tag{18}$$

where $\hat{\mathbf{C}}_l$ and $\mathbf{C}_l$ are the estimated and true locations of the sensor node N_l in the GCS, respectively, L is the set of sensor nodes with the same number of hops h ($h \geq 1$) in a network.

Fig. 5 depicts the simulated results of ρ with various hops and AoA measurement errors in 2-D and 3-D spaces, respectively. We assume the AoA measurement errors follow Normal distribution with zero mean and σ_A as the standard deviation. The fitting curves in Fig. 5 match the simulation results well. We express the fitting curves by a power formula

$$\hat{\rho}(h, \sigma_A) = ah^b + c \tag{19}$$

where $\hat{\rho}$ is the estimated ρ by (19), and parameters a, b and c are related to each σ_A. According to the results in Fig. 5, we generate a lookup table for parameters a, b and c in Table 1. Although the parameter ρ varies with each σ_A, Table 1 only gives rough values of a, b and c with sever ranges of σ_A according to the fitting curves in Fig5. For example, we use the fitting curve of $\sigma_A = 10°$ in Fig5 to generate parameters a, b and c with σ_A in the range of 7.5° to 12.5°
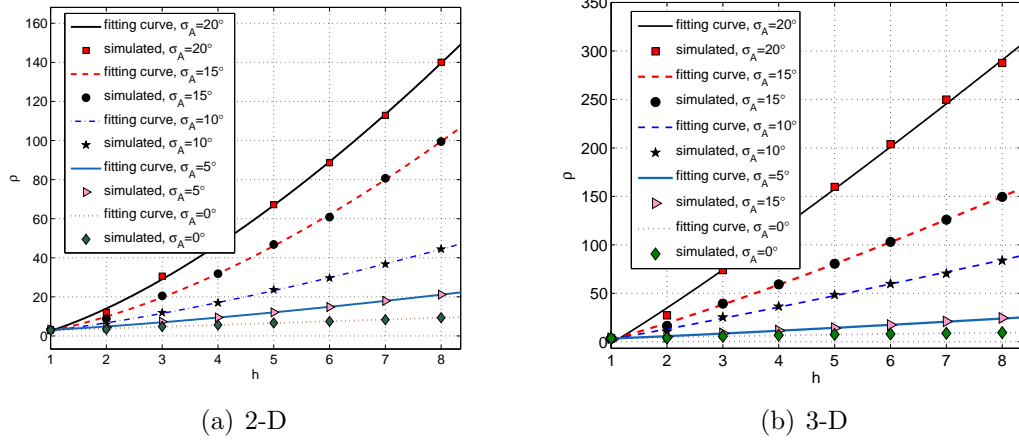
(a) 2-D   (b) 3-D

Figure 5. Estimation errors ρ with increasing hops and their fitting curves.

We define weight on the tth referred anchor node from which the sensor node has h_t hops as

$$w_t = \frac{1}{\hat{\rho}_t(h_t, \sigma_A)} \tag{20}$$

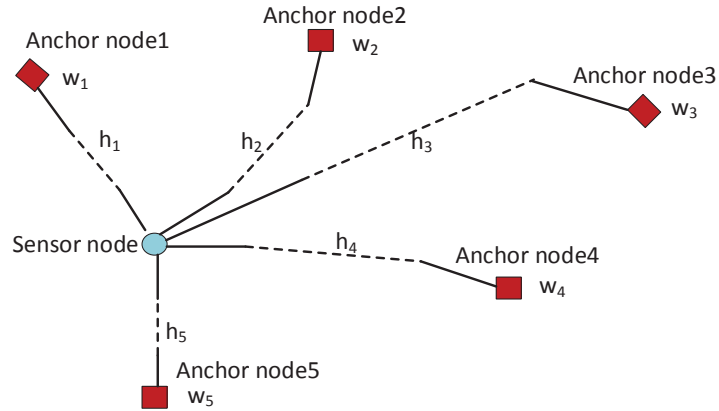In the example of Fig. 6, the sensor node has 5 anchor nodes available, each of which

Figure 6. Localization with mix-hop anchor nodes.

responses different number of hops, resulting in different weights. Note that an anchor node might has different weights with respect to different sensor nodes. The general

form of weighed LS is given by [23]

$$\mathbf{c} = (\mathbf{H}^T \mathbf{W} \mathbf{H})^{-1} \mathbf{H}^T \mathbf{W} \mathbf{B} \tag{21}$$

where $\mathbf{W}$ is the weighting matrix that is diagonal with diagonal elements $[\mathbf{W}]_{tt} = w_t$.

4. SIMULATION RESULTS

In this section, we evaluate the proposed localization method and compare its performance with existing multi-hop localization methods by numerous simulations.

In our simulations, 200 nodes are randomly distributed in a 100×100 m^2 region (2-D) or a $100 \times 100 \times 100$ m^3 region (3-D). The anchor node ratio is 10%. We assume the errors of AoA and distance measurements between neighboring nodes follow Normal distributions with zero mean and σ_A and σ_d as the standard deviations for distance and angle measurements, respectively. σ_A is a certain value of angle and σ_d is a percentage of the real distance. Besides our methods, we also simulated DV-hop, DV-distance, the Euclidean method, the Cosine-law method, the Distance-based method for comparisons.

Three performance metrics are considered in this paper: *distance error*, *localiz -ation error* and *localization coverage*. The distance estimation error is defined as the difference of the estimated distance and the true distance between an anchor node to a sensor node. The distance estimation affects the localization accuracy. Localization error is defined as the Euclidean distance of the real position and estimated position of a sensor node. The localization coverage is the ratio of the number of localizable sensor nodes to the total number of sensor nodes in a network.

4.1. Distance error. Fig. 7 plots the average distance errors of the multi-hop localization methods with communication range of 15 m in 2-D space and 30m in 3-D space, respectively. Since DV-hop[10], DV-distance[10] , Euclidean method[10],

and the Distance-based method [14] do not use AoA measurements, they are immune to AoA measurement errors and σ_A has no impact on them. On the other hand, our proposed method and the Cosine-law method[13] rely on AoA measurements. Therefore, multiple curves with different σ_A are shown in Fig. 7(b). We can observe that our method has lower distance error than DV-hop, DV-distance, and the Distance-based method with σ_A less than a certain value of angle. The Euclidean method has the similar performance with our proposed method when $\sigma_A = 0°$. Fig. 7(b) shows distance errors with various σ_A for our proposed method and the Cosine-law method. Our proposed method always has lower distance errors than the Consine-law method, especially When σ_A and σ_d are relatively large. In other words, our proposed method is more robust than the Consine-law method.
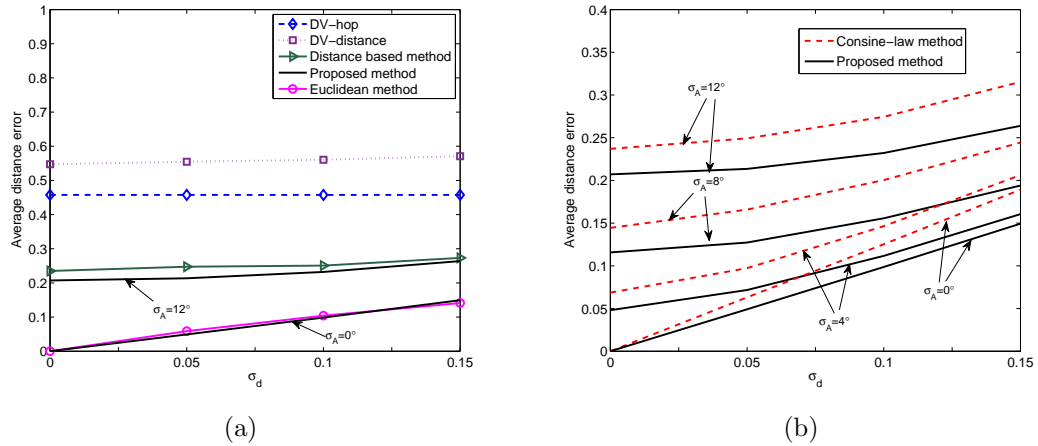

Figure 7. Average distance errors of several in 2-D space.

The average distance errors in 3-D space for DV-hop, DV-distance, the Distance-based method, and our proposed method are depicted in Fig. 8. Our proposed method reaches much lower distance errors than the others. Even when $\sigma_A = 12°$, the distance error of our proposed method is only almost half of that of the Distance-based method.
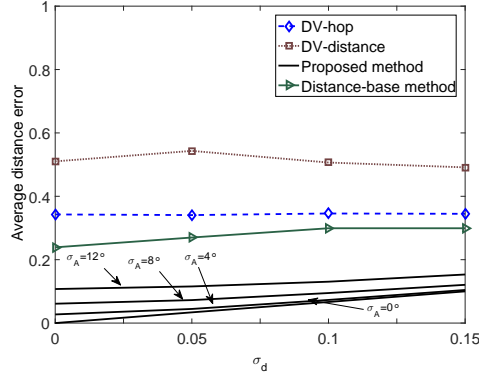
Figure 8. Average distance errors in 3-D space.

4.2. Localization error. Fig. 9 and Fig. 10 depicts average localization errors of these multi-hop localization methods in 2-D and 3-D spaces with various σ_d and σ_A. The communication ranges are 15 m in 2-D space and 30 m in 3-D space. We can observe that our proposed method outperforms all other methods in terms of localization errors. Note that below some point of σ_d, if σ_A is relative large, the Euclidean method has better performance than our method. For example in Fig. 9, when $\sigma_A = 12°$, the Euclidean method has lower localization error with σ_d less than 0.03. However, the average localization error of the Euclidean method grows dramatically with increasing σ_d although the growth rate of its distance error is much slower. This is reasonable since the localization accuracy not only relies on distance estimations but also on the available number of anchor nodes that a sensor node has distance estimations to. The Euclidean method require more neighbors around a sensor node to estimate the distance to an anchor node, which results in fewer anchor nodes available to a sensor node to be located. The fewer available anchor nodes a sensor node has, the larger the localization error is. We also note that our method always has smaller localization errors than the Cosine method no matter what σ_A or σ_d is. The localization performances in 3-D space for the DV-hop, DV-distance, the
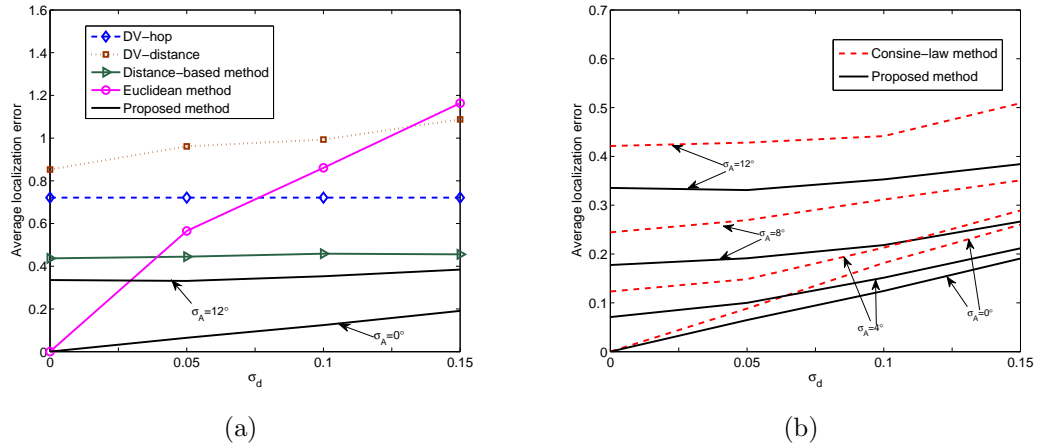
Figure 9. Average localization errors in 2-D.

Distance-based methods, and our proposed method are depicted in Fig. 10. Like in 2-D space, our proposed method has the best performance in terms of localization accuracy.
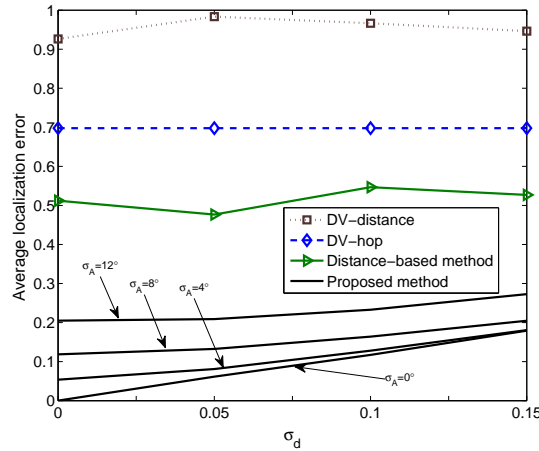

Figure 10. Average localization errors in 3-D.

Our proposed method added weights on anchor nodes to improve localization accuracy based on Table 1. The localization errors with and without weights are shown in Fig. 11. We observe that when the AoA measurement error is small, adding weights dose not make big difference. However when σ_A is relatively large, the lo-

calization accuracy is improved remarkably by adding weights on anchor nodes. For example, in 3-D space, the localization error with weights is about 20% lower than that without weights when $\sigma_A = 12°$.
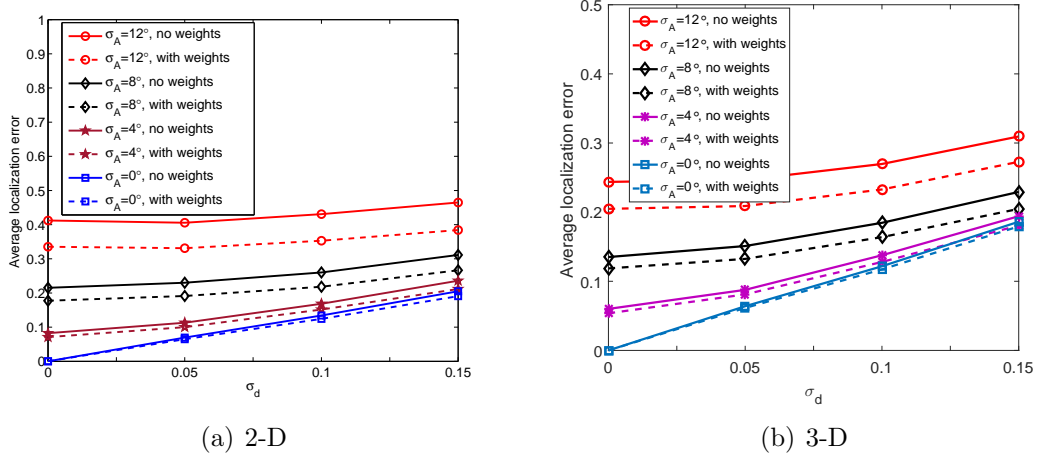

(a) 2-D   (b) 3-D

Figure 11. Average localization errors with and without weights.

4.3. Localization coverage. Fig. 12 shows the performances of these multi-hop localization methods in terms of localization coverage in 2-D and 3-D spaces, respectively. The communication range varies from 6 m to 12 m in 2-D space and from 12 m to 22 m in 3-D space. All localization coverages increase monotonically with the increasing communication range. We observe that the localization coverages of the DV-hop, DV-distance, the Distance-based method, the Cosine-law method and our proposed method almost overlap in 2-D space and are much higher than that of the Euclidean method. It is reasonable since any node which can be located by the DV-hop, DV-distance, the Distance-based method, and the Cosine-law method can also be located by our proposed method in 2-D space. However, the Euclidean method requires more neighboring nodes around a sensor node to be located, which results in lower localization coverage. When the communication ranges of DV-hop, DV-distance, the Distance-based method, the Cosine-law method and our proposed method are relatively large, the localization coverages reach a relatively large value

and the growth rate becomes slower after that. For example, in Fig. 12(a), the localization coverages reach 80% when the communication range is 9 m and the localization coverages do not increase that fast after that.

We also observe that the localization coverage of our proposed method in 3-D space is lower than that of DV-hop, DV-distance, and the Distance-based method, as shown in Fig. 12(b) . In 3-D space, our method requires at least one additional common neighboring node around the to-locate sensor node to estimate the rotation matrix between two LCSs. In other words, some sensor nodes that can be located by DV-hop, DV-distance, and the Distance-based method could not be located by the proposed method in 3-D space, which results in lower localization coverage. However, this sacrifice is worthy since our proposed method can improve the distance and localization accuracy remarkably, as shown in Fig. 8 and Fig. 10.
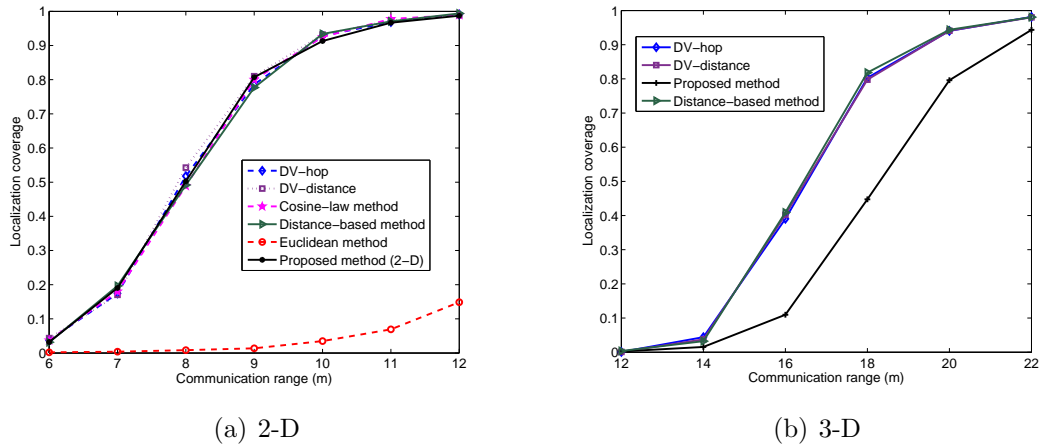

(a) 2-D

(b) 3-D

Figure 12. Localization coverage with various communication ranges.

5. CONCLUSION

In this paper, we proposed a node localization method for underwater wireless sensor network in 2-D and 3-D spaces, where only a small number of anchor nodes are available. To localization sensor nodes in UWSNs, distances from sensor nodes to

anchor nodes are estimated. The whole localization process consists of two phases: distance estimations by multi-hop propagation and tri-lateration localization. We also derived the formulas of weights which are added on anchor nodes according to AoA measurement errors and the number of hops to improve localization accuracy. Numerous simulations are done to verify and compare our proposed method with the existing multi-hop localization methods. Simulation results show that our method can achieve high distance and localization accuracy. Besides, our methods can reach the same high localization coverage as DV-hop, DV-distance, the Distanc-base method, and the Consine-law method in 2-D space, even though the localization coverage gets relatively lower in 3-D space. And the proposed method of calculating weights are proved to be effective, especially when measurement errors are large.

REFERENCES

[1] M. Garcia, S. Sendra, M. Atenas, and J. Lloret, "Underwater wireless ad-hoc networks: A survey," *Mobile ad hoc networks: Current status and future trends*, pp. 379–411, 2011.

[2] D. Niculescu and B. Nath, "Ad hoc positioning system (aps) using aoa," in *INFOCOM 2003. Twenty-Second Annual Joint Conference of the IEEE Computer and Communications. IEEE Societies*, vol. 3. IEEE, 2003, pp. 1734–1743.

[3] J. Kong, J.-h. Cui, D. Wu, and M. Gerla, "Building underwater ad-hoc networks and sensor networks for large scale real-time aquatic applications," in *Military Communications Conference, 2005. MILCOM 2005. IEEE.* IEEE, 2005, pp. 1535–1541.

[4] V. Chandrasekhar, W. K. Seah, Y. S. Choo, and H. V. Ee, "Localization in underwater sensor networks: survey and challenges," in *Proceedings of the 1st ACM international workshop on Underwater networks.* ACM, 2006, pp. 33–40.

[5] J.-E. Garcia, "Ad hoc positioning for sensors in underwater acoustic networks," in *OCEANS'04. MTTS/IEEE TECHNO-OCEAN'04*, vol. 4. IEEE, 2004, pp. 2338–2340.

[6] I. F. Akyildiz, P. Wang, and Z. Sun, "Realizing underwater communication through magnetic induction," *IEEE Communications Magazine*, vol. 53, no. 11, pp. 42–48, 2015.

[7] H.-P. Tan, R. Diamant, W. K. Seah, and M. Waldmeyer, "A survey of techniques and challenges in underwater localization," *Ocean Engineering*, vol. 38, no. 14, pp. 1663–1676, 2011.

[8] H. Huang, Y. R. Zheng, and W. Duan, "Pseudo-noise based time of arrival estimation for underwater acoustic sensor localization," in *OCEANS 2016-Shanghai*. IEEE, 2016, pp. 1–5.

[9] Z. Zhou, Z. Peng, J.-H. Cui, Z. Shi, and A. Bagtzoglou, "Scalable localization with mobility prediction for underwater sensor networks," *IEEE Transactions on Mobile Computing*, vol. 10, no. 3, pp. 335–348, 2011.

[10] D. Niculescu and B. Nath, "Ad hoc positioning system (aps)," in *Global Telecommunications Conference,*, vol. 5. IEEE, 2001, pp. 2926–2931.

[11] M. Erol, L. F. M. Vieira, and M. Gerla, "AUV-aided localization for underwater sensor networks," in *Wireless Algorithms, Systems and Applications, International Conference*. IEEE, 2007, pp. 44–54.

[12] Z. Zhou, J.-H. Cui, and S. Zhou, "Localization for large-scale underwater sensor networks," in *International Conference on Research in Networking*. Springer, 2007, pp. 108–119.

[13] Z. Zhu, W. Guan, L. Liu, S. Li, S. Kong, and Y. Yan, "A multi-hop localization algorithm in underwater wireless sensor networks," in *Wireless Communications and Signal Processing (WCSP), 2014 Sixth International Conference on*. IEEE, 2014, pp. 1–6.

[14] N. H. Will and J. Schiller, "Distance-based distributed multihop localization in mobile wireless sensor networks," *8th GI/ITG KuVS Fachgesprch Drahtlose Sensornetze (FGSN'09)*, vol. 34, 2009.

[15] A. G. Zajić, "Statistical modeling of MIMO mobile-to-mobile underwater channels," *Vehicular Technology, IEEE Transactions on*, vol. 60, no. 4, pp. 1337–1351, 2011.

[16] L. E. Emokpae, S. DiBenedetto, B. Potteiger, and M. Younis, "Ureal: underwater reflection-enabled acoustic-based localization," *IEEE Sensors Journal,*, vol. 14, no. 11, pp. 3915–3925, 2014.

[17] Z. Liu, H. Gao, W. Wang, S. Chang, and J. Chen, "Color filtering localization for three-dimensional underwater acoustic sensor networks," *Sensors*, vol. 15, no. 3, pp. 6009–6032, 2015.

[18] W. A. van Kleunen, K. C. Blom, N. Meratnia, A. B. Kokkeler, P. J. Havinga, and G. J. Smit, "Underwater localization by combining time-of-flight and direction-of-arrival," in *OCEANS 2014-TAIPEI*. IEEE, 2014, pp. 1–6.

[19] L. E. Emokpae and M. Younis, "Throughput analysis for shallow water communication utilizing directional antennas," *IEEE Journal on Selected Areas in Communications*, vol. 30, no. 5, pp. 1006–1018, 2012.

[20] O. Sorkine, "Least-squares rigid motion using SVD," *Technical notes*, vol. 120, no. 3, p. 52, 2009.

[21] T. Bian, R. Venkatesan, and C. Li, "Design and evaluation of a new localization scheme for underwater acoustic sensor networks," in *Global Telecommunications Conference.* IEEE, 2009, pp. 1–5.

[22] Y. Han, Y. R. Zheng, and D. Sun, "Measurement error impact on node localization of large scale underwater sensor networks," in *Vehicular Technology Conference (VTC Fall), 2015 IEEE 82nd.* IEEE, 2015, pp. 1–5.

[23] S. M. Kay, *Fundamentals of statistical signal processing: Estimation theory.* Englewood Cliffs, NJ: Prentice-Hall, 1993.

III. AOA ASSISTED LOCALIZATION FOR UNDERWATER AD-HOC SENSOR NETWORKS

Huai Huang and Yahong Rosa Zheng

Department of Electrical & Computer Engineering

Missouri University of Science and Technology

Rolla, Missouri 65409–0050

Email: {hh6v8, zhengyr}@mst.edu

ABSTRACT

In this paper, We propose angle of arrival (AoA) assisted localization scheme for underwater Ad-Hoc sensor networks in 2-D and 3-D. This scheme estimates distances from sensor nodes to anchor nodes via multi-hops with the help of AoA measurements. By forwarding distance at each node hop-by-hop, the distance estimations can be flooded to the whole network. Once a sensor node got distance estimations from at least three (in 2-D) or four (3-D) anchor nodes, the location of the sensor node is calculated. Comparing to the existing localization schemes in Ad-Hoc networks: DV-distance, DV-hop, and Euclidean propagation, the simulation results show that our proposed method improves localization accuracy significantly while keeping high localization coverage.

1. INTRODUCTION

Underwater Ad-Hoc sensor networks (UWASNET) have found important applications in ocean exploration, critical structure monitoring, coastal surveillance, and disaster mitigation. For example, the melting process of the polar ice sheets,

which contributes to the sea level rise, calls for an underwater Ad-Hoc network to provide the timely sea level monitoring. Many Ad-Hoc network applications typically require the knowledge of geographic positions of nodes in the network for mobility tracking, routing and coordination purposes. The accuracy and coverage of localization in an UWASNET are our main concerns. The widely used positioning system is the Globe Positioning System (GPS) which is not feasible in underwater because the radio-frequency signals utilized by GPS have very limited communication ranges due to the strong propagation loss in water[1].

The main feature of an Ad-Hoc network is infrastructure-less and a large number of randomly placed nodes with varying capability [2]. The typical UWASNET scenario, which is depicted in Fig. 1, only has a small fraction of nodes with fixed locations, named *anchor* node. Anchor nodes know their absolute positions from GPS or surface buoys. Other nodes called *sensor* node can estimate their own location by communicating with other nodes in their communication range. The nodes in the communication neighborhood of a node are called *neighbors* of this node.
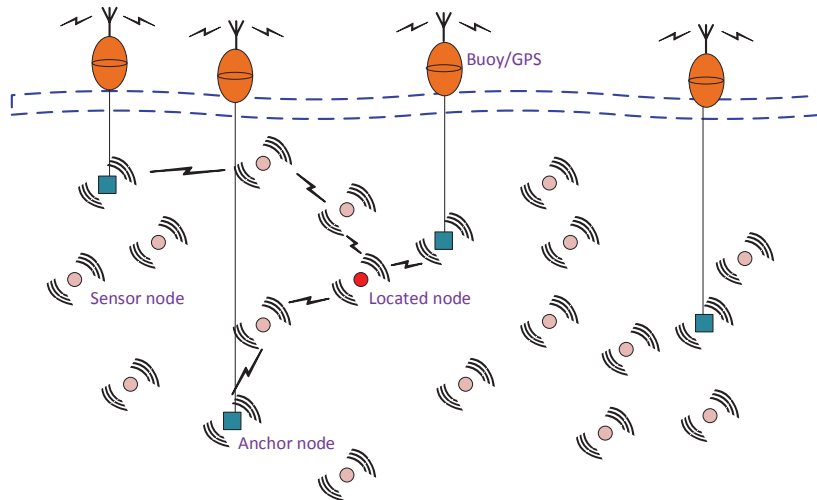

Figure 1. The framework of Underwater Ad-Hoc sensor networks.

The exiting localization schemes in underwater wireless sensor networks are usually classified into two categories: range-based schemes and range-free schemes [3]. Since range-free schemes can only obtain coarse localization, range-based schemes are widely used. Range-based schemes [3], which consist of three phases: distance estimation, position estimation and refinement. Since the communication range is limited in large scale UWASNET, only nodes within a communication neighborhood can obtain distance estimations between each other by communicating directly with neighbors. Therefore, the localization coverage is related to node density of the network. In a dense network, the recursive localization method reaches high localization coverage [4]. However, when the network is sparse, the localization coverage is getting down significantly because recursive localization method requires at least four nodes (in 3-D) with known locations within the communication range of the sensor node that needs to be located. To extend the localization coverage in a sparse network, one option is to forward distance estimation to anchor nodes hop by hop between sensor nodes. This distance information starts at the anchor nodes and is flooded to the whole network.

The paper [5] summarizes three popular algorithms via mulit-hops to estimate distance in Ad-Hoc networks: *DV-hop*, *DV-distance*, and *Euclidean* propagation methods. The DV-hop method employs a classical distance vector (DV) exchange so that sensor nodes in a network estimate distance to anchor nodes in *hops*. DV-distance is similar to DV-hop with the difference that distance between neighbors is propagated in *meters* rather than in *hops*. These two schemes just get coarse localization. Euclidean scheme calculates *Euclidean* distances between sensor nodes and anchor nodes, with higher accuracy of distance estimations. Therefore, Euclidean scheme achieves more accurate localization while with limited localization coverage

when the ratio of anchor nodes is small[5]. This paper aims to increase the accuracy of localization while keeping relative high localization coverage in UWASNET. We propose an angle of arrival (AoA) assisted localization scheme for UWASNET.

Recent work in the field [6] has shown the feasibility of utilizing AoA measurements in underwater networks. The paper [7] utilizes AoA measurements to provide the 3-D ranging estimation in underwater environment. Papers [8, 9] show localization in underwater sensor networks based on AoA. AoA capability is usually achieved by using directional antennas [10] or antenna array. In this paper, we assume each nodes in UWASNET is able to measure the AoA from its neighbors. The simulation results show our proposed scheme can achieve better localization accuracy comparing to DV-hop and DV-distance schemes, with almost the same high localization coverage as these two schemes.

2. EXISTING WORK

2.1. DV-hop. The DV-hop scheme counts distances between nodes in hops. Each node in a network has a hop table $\{h_i\}$ and exchange the table with its neighbors. The hop forwarding starts from a anchor node and floods into the sensor network. When a node receives the hop table from its neighbor, the node updates its own hop table. Once the hop-forwarding hits another anchor node, it estimates the average size of one hop based on the knowledge of the two anchor nodes' absolute locations. A sensor node uses the average size of one hop and its hop table to estimate its distance to anchor nodes in meters. We can see the DV-hop method is simple and is immune to measurement errors. However, it can only provide coarse distance estimations.

2.2. DV−distance. The DV-distance approach is similar to the DV-hop method in terms of the forwarding procedure. The difference lies in that the forwarded distance between nodes is in *meters*, rather than in *hops*. The distance from a anchor node to a sensor node is then calculated by summing up the hop-by-hop

distances. The DV-distance scheme is still coarse because the real distance between a sensor node and a anchor node should be the distance of the line-of-sight, not the cumulative hop-by-hop distance. For example, in Fig. 4, the distance from node $N_0^{[1]}$ to node N_3 estimated by DV-distance is the sum of distances between nodes $N_0^{[1]}$ and N_1, between nodes N_1 and N_2, and between nodes N_2 and N_3.

2.3. Euclidean propagation. The Euclidean method calculates the *Euclidean* distances from sensor nodes to anchor nodes. Therefore, this method provides more accurate distance estimation. However, the Euclidean distance algorithm requires at least two neighbors that has the known distances to a anchor nodes. This requirement restricts the localization coverage.

2.4. AoA theory. Each node in the network has an axis against which the arrival angles from neighbors are reported. After deployment, the axis of a node has arbitrary direction, which is represented by the bold arrow in Fig. 2. The term *bearing* represents the angle measured with respect to a neighbor. In this paper, bearings of each node with respect to neighbors provides AoA estimations. In Fig. 2, for node N_2, the bearing against the axis provides the AoA measurements of $\widehat{n_1n_2}$ and $\widehat{n_3n_2}$ from two neighbors of N_1 and N_3, respectively. With AoAs measured, the included angle at the node can be estimated.
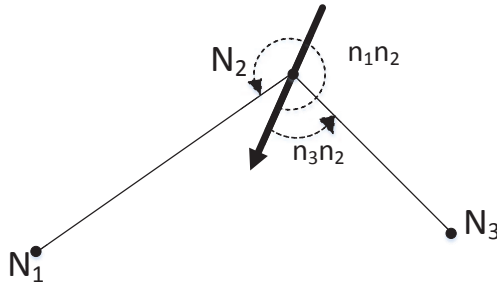

Figure 2. AoAs at a node.

3. THE PROPOSED SCHEME

3.1. AoA assisted localization in 3-D. Without loss of generality, a simple scenario of UWASNET in 3-D is shown in Fig. 3, where nodes of N_1, N_2 and N_3 are sensor nodes. $N_0^{(k)}$ ($k \subseteq [1, K]$) denotes the k-th anchor node in the network, where K is the number of the anchor nodes in the network. So $N_0^{(1)}$ is the first anchor node in the network. Only node N_1 is within the communication range of the first anchor node. Nodes N_2 and N_3 are too far to communicate with node $N_0^{[1]}$ directly. And node N_2 is a neighbor of nodes N_1 and N_3. Node N_3 can only reach node N_2. We call each communication range as one hop. In other words, there are three hops between anchor node $N_0^{[1]}$ and node N_3. Let the hop-count of anchor node equal to 0 and the hop-counts of node N_1, N_2 and N_3 be 1, 2, and 3, respectively. We assume the neighbors in a communication range have the capability of distance measuring between each other by time of arrival (ToA) or time difference of arrival (TDoA) or received signal strength indicator (RSSI). $r_{01}^{(1)}$ in Fig. 3 denotes the distance measured from anchor node $N_0^{(1)}$ to the sensor node N_1. r_{12} is the distance measurement between sensor nodes of N_1 and N_2.

All nodes, equipped with multi-modal directional piezoelectric underwater transducers, can be configured to measure both azimuth and elevation angles [7]. In 3-D, each sensor node has its own local coordinate system with arbitrary orientation and with the sensor node as the origin of the local coordinate system. The AoA of node N_i in the 3-D coordinate system of the node N_j is represent by a vector

$$\mathbf{v}_{ij} = [\theta_{ij}, \phi_{ij}] \qquad i, j \subseteq [1, N] \tag{1}$$

where θ_{ij} denotes elevation angle and ϕ_{ij} represents azimuth angle in the local coordinate system of node j, and N is the number of the sensor nodes in the network. The AoA vector of anchor node $N_0^{(1)}$ at node N_1 is $\mathbf{v}_{01}^{(1)} = [\theta_{01}^{(1)}, \phi_{01}^{(1)}]$, and the AoA

vector at node N_1 from node N_2 are $\mathbf{v}_{21} = [\theta_{21}, \phi_{21}]$. The AoA vectors of sensor nodes N_3 and node N_1 at node N_2 are $\mathbf{v}_{32} = [\theta_{32}, \phi_{32}]$ and $\mathbf{v}_{12} = [\theta_{12}, \phi_{12}]$, which are shown in in Fig. 3.
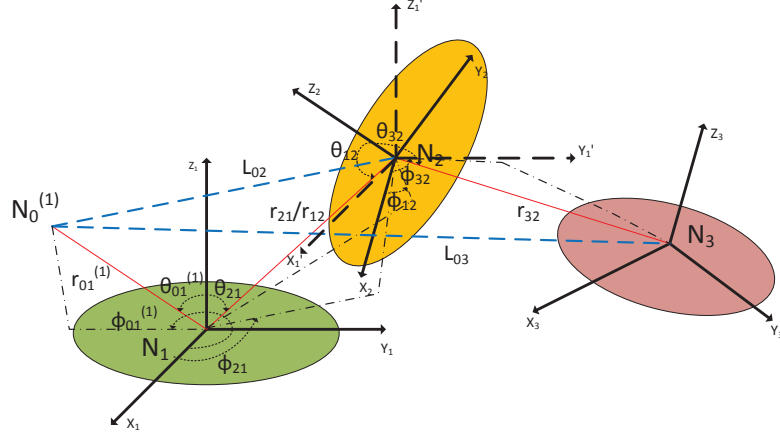

Figure 3. AoA assisted distance estimation in 3-D network with multiple nodes.

According to the transform of Spherical Coordinate System (SCS) to Rectangular Coordinate System (RCS), the rectangular coordinates of anchor node $N_0^{(1)}$ ($\mathbf{A}_{01}^{(1)}$) in the local RCS $X_1 Y_1 Z_1$ is defined as

$$\mathbf{A}_{01}^{(1)} = [x_{01}^{(1)}, y_{01}^{(1)}, z_{01}^{(1)}]^T \tag{2}$$

where $[]^T$ represents transpose of a matrix and $x_{01}^{(1)}$, $y_{01}^{(1)}$, $z_{01}^{(1)}$ are calculated as

$$x_{01}^{(1)} = r_{01}^{(1)} \sin \theta_{01}^{(1)} \cos \phi_{01}^{(1)}$$
$$y_{01}^{(1)} = r_{01}^{(1)} \sin \theta_{01}^{(1)} \sin \phi_{01}^{(1)} \tag{3}$$
$$z_{01}^{(1)} = r_{01}^{(1)} \cos \theta_{01}^{(1)}$$

For the same reason, the rectangular coordinates $\mathbf{A}_{21}$ of node N_2 in the RCS $X_1 Y_1 Z_1$ is expressed as

$$\mathbf{A}_{21} = \left[x_{21}, y_{21}, z_{21} \right]^T \tag{4}$$

where y_{L11}, z_{L11} are calculated as

$$x_{21} = r_{21} \sin \theta_{21} \cos \phi_{21}$$

$$y_{21} = r_{21} \sin \theta_{21} \sin \phi_{21} \tag{5}$$

$$z_{21} = r_{21} \cos \theta_{21}$$

Once the the rectangular coordinates of anchor node $N_0^{(1)}$ and node N_2 are gotten in the RCS $X_1 Y_1 Z_1$, the distance between these two nodes $L_{02}^{(1)}$ is calculated by

$$L_{02}^{(1)} = \|\mathbf{A}_{21} - \mathbf{A}_{01}^{(1)}\| \tag{6}$$

where $\|\cdot\|$ denotes the vector norm. Substituting equations (2)-(5) into equation (6), node N_2 with 2 hops gets its distance estimation from anchor node $N_0^{(1)}$.

The next step is to estimate the distances of nodes with hop-count more than 2 to anchor nodes, like the distance from node N_3 to anchor node $N_0^{(1)}$ $L_{03}^{(1)}$. The main idea is to find the rectangular coordinates of the sensor node and the anchor node with respect to the same RCS of another node. For example, the distance $L_{03}^{(1)}$ is obtainable once the coordinates of node N_3 and nchor node $N_0^{(1)}$ are found in the local N_2 RCS. The coordinates of node N_3 $\mathbf{A}_{32}$ in the N_2 RCS is easy to calculate because node N_3 is a neighbor of node N_2. However, the coordinates of the landmark $N_0^{(1)}$ $\mathbf{A}_{02}^{(1)}$ in N_2 RCS cannot be calculated by communicating directly between these two nodes because they are not located within a neighborhood. To get coordinate $\mathbf{A}_{02}^{(1)}$, we first calculate the coordinates of node N_1 in N_2 RCS, denoted as $\mathbf{A}_{12}$. Since

node N_1 can communicate directly with node N_2, the coordinates $\mathbf{A}_{12}$ is expressed as

$$x_{12} = r_{12} \sin\theta_{12} \cos\phi_{12}$$

$$y_{12} = r_{12} \sin\theta_{12} \sin\phi_{12} \tag{7}$$

$$z_{12} = r_{12} \cos\theta_{12}$$

If we parallel shift the origin of the RCS $X_1 Y_1 Z_1$ to node N_2, as shown by the thick dash lines in Fig. 3, then, the RCS $X_2' Y_2' Z_2'$ has the same orientation of the RCS $X_1 Y_1 Z_1$ while having node N_2 as the origin. Therefore, the coordinates of node N_1 in RCS $X_2' Y_2' Z_2'$, denoted as $\mathbf{A}_{12}'$, satisfies

$$\mathbf{A}_{12}' = \text{-}\mathbf{A}_{21} \tag{8}$$

It is noticed that RCS $X_2' Y_2' Z_2'$ is a rotation of RCS $X_2 Y_2 Z_2$ with the same origin. Let $\mathbf{R}_{12}$ be the rotation matrix of these two RCSs in node N_2 with 3×3 dimensions.

$$\mathbf{A}_{12} = \mathbf{R}_{12}\mathbf{A}_{12}' \tag{9}$$

Therefore, the rotation matrix can then be determined by

$$\mathbf{R}_{12} = \mathbf{A}_{12}(\mathbf{A}_{12}'^{T}\mathbf{A}_{12}')^{-1}\mathbf{A}_{12}'^{T} \tag{10}$$

The coordinates of a node in RCS $X_1 Y_1 Z_1$ can be transformed into coordinates in RCS $X_2 Y_2 Z_2$ with considering the origin difference and rotation matrix between these two RCS. The coordinate of anchor node $N_0^{(1)}$ in RCS $X_2 Y_2 Z_2$ $\mathbf{A}_{02}^{(1)}$ is expressed as

$$\mathbf{A}_{02}^{(1)} = \mathbf{R}_{12}\mathbf{A}_{01}^{(1)} + (-\mathbf{A}_{12}) \tag{11}$$

where $-\mathbf{A}_{12}$ is considered as the original point offset. Substituting equation (8) and (10) into equation (11), coordinates $\mathbf{A}_{02}^{(1)}$ is calculated. The distance between anchor node $N_0^{(1)}$ and node N_3 is then shown below

$$L_{03}^{(1)} = \|\mathbf{A}_{02}^{(1)} - \mathbf{A}_{32}\| \tag{12}$$

With the same method, the distance estimation can be flooded to more nodes with higher hop-count in the whole network. Once a sensor node obtain distances to more than 4 anchor nodes (in 3-D) or 3 anchor nodes (in 2-D), its position is calculated by using trilateration algorithm, like the located node in Fig. 1. With more anchor nodes available, Least Squares method is usually used to optimize the location estimation [11].

3.2. AoA assisted localization in 2-D. Sometimes, we just need localization in 2-D in underwater because the depth can be obtained by using pressure sensors. Localization procedure in 2-D is Just like the localization algorithm in 3-D, with the parameter $\theta_{ij} = \pi/2$. We also should note that the rotation matrix is 2×2 dimensions, instead of 3×3 dimensions in 3-D.

We introduce another straightforward scheme to localization in 2-D in this section. This method is based on the law of cosines to calculate distances rather than coordinates transformation in different RCS used in 3-D localization.

A node, from which the hop-count of a neighbor node is derived, is called *prior* node of the neighbor node. In turn, the node whose hop-count is derived is termed as *posterior* node. For example, for node N_2, nodes N_1 and N_3 are the prior and posterior nodes.

Any node that has two communication neighbors is able to obtain its included angle between these two neighbors by using AoA measurements [2]. For example, the include angle at node N_2 with respect to nodes N_1 and N_3 is obtainable as long as
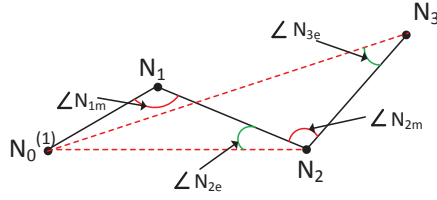
Figure 4. Basic principle of AoA assisted distance estimation in 2-D.

node N_2 receives the AoAs from nodes N_1 and N_3. This included angle at a node between the prior node and posterior node is termed as *mearsued-angle* of this node. For example, the measured-angle of node N_2 in Fig. 4 is $\angle N_{2m}$. The distance between nodes N_2 and $N_0^{[1]}$ is inferred according to the law of cosines, with the angle $\angle N_{1m}$ and distances of $L_{01}^{[1]}$ and L_{12}, which is shown in equation (13).

$$L_{02}^{[1]} = \sqrt{\{L_{01}^{[1]2} + L_{12}^2 - 2L_{01}^{[1]}L_{12}\cos(\angle N_{1m})\}} \tag{13}$$

Therefore, the node N_2 with the hop-count of 2 obtains its distance estimation to the anchor node. Once $L_{02}^{[1]}$ is calculated, the angle $\angle N_{2e}$ in Fig. 4, which is called *estimated-angle* at node N_2, is acquirable based on the law of cosines.

$$\angle N_{2e} = \arccos\left\{\frac{L_{02}^{[1]2} + L_{12}^2 - L_{01}^{[1]2}}{L_{02}^{[1]}L_{12}}\right\} \tag{14}$$

For node N_3, the distance $L_{03}^{[1]}$ is calculated based on the knowledge of $L_{02}^{[1]}$, L_{23}, $\angle N_{2e}$ and $\angle N_{2m}$.

$$L_{03}^{[1]} = \sqrt{L_{02}^{[1]2} + L_{23}^2 - 2L_{02}^{[1]}L_{23}\cos(\angle N_{2m} \pm \angle N_{2e})} \tag{15}$$

With the same method, nodes with higher hop-counts can get the distance estimations from anchor nodes.

4. SIMULATION RESULTS

In this section, we simulate the proposed propagation method, DV-hop, and DV-distance and compare their performances.

In our simulation, 100 sensor nodes are randomly distributed in a 20×20 Km^2 region. The anchor node ratio is 5%. The node degree is defined as the expected number of nodes in a communication neighborhood. The node degree is controlled by changing the communication range R. The errors of AoA and distance measurements in a neighborhood follow normal distributions, with zero as mean values and standard deviations σ to be some percents of the real angles and distances.

Three performance metrics are considered in this paper: distance estimation error, localization error and localization coverage. The distance estimation error is defined as the difference between the real distance and the estimated distance of a sensor node to anchor nodes, which affects the localization accuracy. Localization error is defined as the average distance of the real positions and estimated positions of nodes. The localization coverage is the ratio of number of located nodes to the total number of sensor nodes in the network.

The cumulative distribution of estimated distance errors is demonstrated in Fig. 5 with σ of 0.1, 0.05, and 0.01, respectively. The communication range is set as $R = 5Km$. The distance errors are normalized by the communication range.

We notice from Fig. 5 that our proposed scheme has smaller estimated distance errors than DV-hop and DV-distance methods. For example, for $\sigma = 0.05$, 90% of the trails of our proposed algorithm have distance errors within 7.6% of the communication range. In contrast, the distance errors for DV-hop and DV-distance reach to 23% and 27% of the communication range for 90% of the trails. However, our proposed method and DV-distance method corrupt with increasing measure error of distances and angles. DV-hop method is immune to measure error.
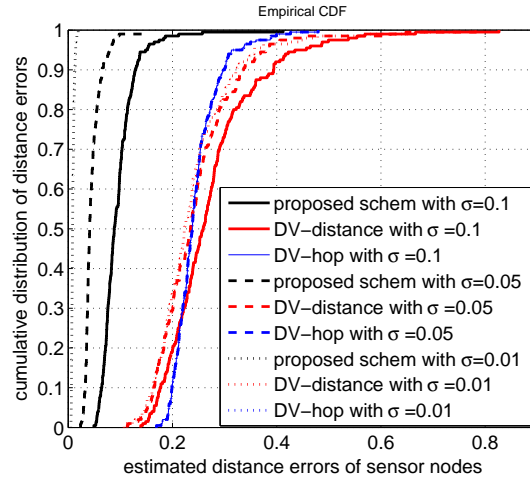
Figure 5. Cumulative estimation of distance errors to anchor nodes with different σ.

Fig. 6 shows the distance error distribution with different communication rang R or different node degrees. The standard deviation of measurement σ=0.05. The performance of our propose algorithm is still the best, and get worse with the decreased communication range R. The DV-distance method suffers more from the decreasing R. The performance of DV-distance even becomes worse than DV-hop method when R is getting smaller.
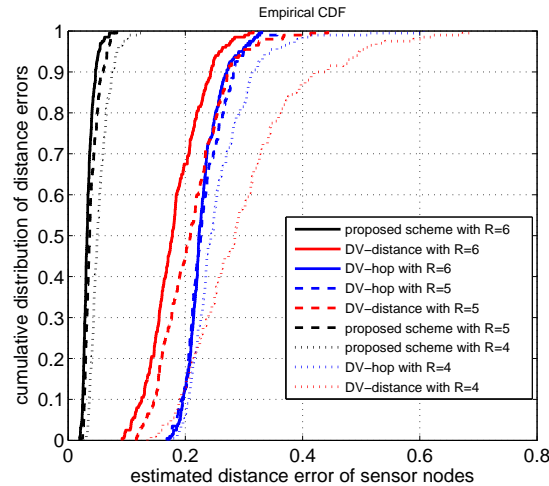

Figure 6. Cumulative estimation of distance errors to landmarks with different R.

The localization coverage of DV-hop, DV-distance and the proposed scheme is depicted in Fig. 7, where the three curves almost overlap. Therefore, the proposed algorithm achieves as high coverage as DV-hop and DV-distance.
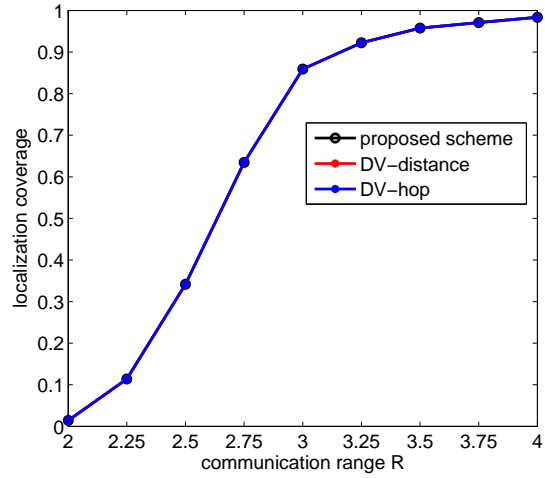

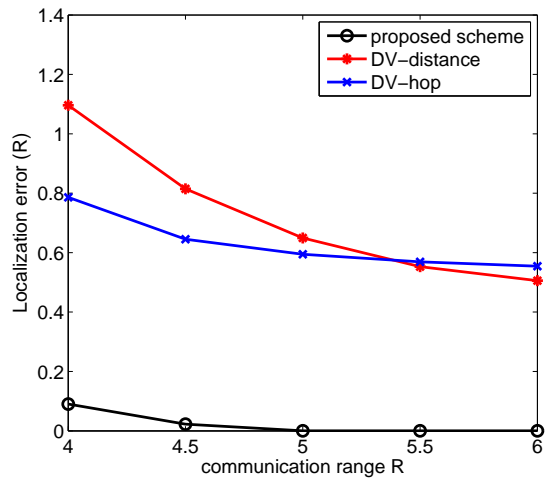Figure 7. Location coverage with different R.

Figure 8. Location error with different R.

Fig. 8 plots the localization error versus communication range R. The σ is set to be 0.05. It is observed that our proposed method has much smaller localization errors comparing to DV-hop and DV-distance methods. When the communication range increases, the location error is getting smaller. The significant improvement of location accuracy is the main advantage of our propose method.

5. CONCLUSION

In this paper, this paper proposed an AoA assisted localization scheme for underwater Ad-Hoc networks in 2-D and 3-D, where only a small fraction of anchor nodes are available. To localization sensor nodes in UWANET, distances from sensor nodes to anchor nodes are estimated. Comparing with DV-hop and DV-distance algorithms, our proposed scheme can improve the accuracy of localization significantly. What's more, the localization coverage of our scheme keep as high as DV-hop and DV-distance algorithms.

REFERENCES

[1] J.-E. Garcia, "Ad hoc positioning for sensors in underwater acoustic networks," in *OCEANS'04. MTTS/IEEE TECHNO-OCEAN'04*, vol. 4. IEEE, 2004, pp. 2338–2340.

[2] D. Niculescu and B. Nath, "Ad hoc positioning system (aps) using aoa," in *IN-FOCOM 2003. Twenty-Second Annual Joint Conference of the IEEE Computer and Communications. IEEE Societies*, vol. 3. Ieee, 2003, pp. 1734–1743.

[3] H.-P. Tan, R. Diamant, W. K. Seah, and M. Waldmeyer, "A survey of techniques and challenges in underwater localization," *Ocean Engineering*, vol. 38, no. 14, pp. 1663–1676, 2011.

[4] Z. Zhou, J.-H. Cui, and S. Zhou, "Localization for large-scale underwater sensor networks," in *International Conference on Research in Networking*. Springer, 2007, pp. 108–119.

[5] D. Niculescu and B. Nath, "Ad hoc positioning system (aps)," in *Global Telecommunications Conference, 2001. GLOBECOM'01. IEEE*, vol. 5. IEEE, 2001, pp. 2926–2931.

[6] A. G. Zajić, "Statistical modeling of mimo mobile-to-mobile underwater channels," *Vehicular Technology, IEEE Transactions on*, vol. 60, no. 4, pp. 1337–1351, 2011.

[7] L. E. Emokpae, S. DiBenedetto, B. Potteiger, and M. Younis, "Ureal: underwater reflection-enabled acoustic-based localization," *Sensors Journal, IEEE*, vol. 14, no. 11, pp. 3915–3925, 2014.

[8] Z. Liu, H. Gao, W. Wang, S. Chang, and J. Chen, "Color filtering localization for three-dimensional underwater acoustic sensor networks," *Sensors*, vol. 15, no. 3, pp. 6009–6032, 2015.

[9] W. A. van Kleunen, K. C. Blom, N. Meratnia, A. B. Kokkeler, P. J. Havinga, and G. J. Smit, "Underwater localization by combining time-of-flight and direction-of-arrival," in *OCEANS 2014-TAIPEI*. IEEE, 2014, pp. 1–6.

[10] L. E. Emokpae and M. Younis, "Throughput analysis for shallow water communication utilizing directional antennas," *IEEE Journal on Selected Areas in Communications*, vol. 30, no. 5, pp. 1006–1018, 2012.

[11] T. Bian, R. Venkatesan, and C. Li, "Design and evaluation of a new localization scheme for underwater acoustic sensor networks," in *Global Telecommunications Conference, 2009. GLOBECOM 2009. IEEE*. IEEE, 2009, pp. 1–5.

IV. PSEUDO-NOISE BASED TIME OF ARRIVAL ESTIMATION FOR UNDERWATER ACOUSTIC SENSOR LOCALIZATION

Huai Huang, Weiming Duan, and Yahong Rosa Zheng

Department of Electrical & Computer Engineering

Missouri University of Science and Technology

Rolla, Missouri 65409–0050

Email: {hh6v8, zhengyr}@mst.edu

ABSTRACT

This paper compares the performance of single pseudo-noise (PN) and dual PN (DPN) sequences for time of arrival (ToA) estimation in underwater acoustic (UWA) localization. The single PN scheme uses the correlation of a local PN sequence and the received PN signal to estimate the ToA. The DPN scheme utilizes the cross correlation of the two received PN segments in one signal frame to calculate the ToA. Both simulation and field test results show that the DPN design outperforms the single PN scheme, as the DPN scheme is robust to the severe underwater acoustic channel dispersion and the high carrier frequency offset (CFO) in low-cost hardware systems where the atomic clock is unavailable.

1. INTRODUCTION

Underwater wireless sensor networks (UWSN) have found important applications in ocean exploration, critical structure monitoring, coastal surveillance, and disaster mitigation. In these applications, sensing information is often tagged with time and locations that can be used for tracking nodes and coordinating motion [1].

For example, bridge scour monitoring is made possible with "smart rocks" that are equipped with acoustic transceivers and sensors, and anchor nodes near the river banks utilize the acoustic communication signals to locate the sensor nodes in water [2].

The exiting localization schemes in underwater wireless sensor networks are usually classified into two categories: range-based schemes and range-free schemes [3]. Since range-free schemes can only obtain coarse localization, range-based schemes are widely used. In the range-based approaches, the distance is measured by several schemes: received signal strength indicator (RSSI), time difference of arrival (TDoA) and time of arrival (ToA) [4]. Most range-based localization schemes use ToA or TDoA due to the slow sound propagation in underwater (1500 m/s) and the ToA and TDoA schemes can achieve better accuracy than the RSSI schemes [3]. In this paper, we investigate low cost ToA estimation methods using pseudo noise (PN) sequences. We identify two challenges when these PN based ToA estimation methods are applied in practical underwater localization system.

First, the ToA estimation is sensitive to the dispersion in underwater acoustic (UWA) channels. Typically, UWA channels exhibit severe multipath fading and Doppler spread that arises from nodes or water motion [5]. For example, the multipath delay in the shallow water channel is typically at the level of several tens milliseconds. Moreover, the direct path may not exhibit the strongest energy, which results in the ambiguity for the arrival time estimation. The experimental results in [2] have shown that ToA estimations fluctuated due to the severe multipath spread in the UWA channels.

Second, the high carrier frequency offset (CFO) in the low cost hardware system may greatly lower the accuracy of PN based ToA estimation. The single PN based design was initially implemented on a DSP platform with high performance piezo-electrical crystal oscillator [2]. To further lower the hardware cost and power

consumption, we investigate a new PN based localization system with cheap and low power consumption MCU (Micro-controller Unit) and oscillator. We identify a major challenge in the low cost ToA estimation design: the cheap oscillator in the low cost design has unstable carrier frequency, which results in high carrier frequency offset (CFO), up to 1800 PPM (Parts Per Million). Through simulation and field test, we find that the high CFO greatly degrades the accuracy of the traditional PN based ToA estimation.

We evaluate two PN based schemes for the ToA estimation under these two challenges: dual PN (DPN) scheme and single PN scheme. The DPN signal frame consists of two identical PN sequences separated by some gaps. We calculate the cross correlation of the two PN segments in the received DPN frame, rather than the correlation of the received single PN and a local PN, which is used in the single PN scheme. Therefore, the dual PN based approach has two advantages over the single PN method. First, the cross correlation operation in the dual PN method could focus the multipath signal, which is capable of combatting the multipath effect in the UWA channels. Second, since the cross correlation is operated with two segments of the received PN signals, the high CFO has no influence on the ToA estimation accuracy in the low cost transceiver system where cheap system clocks are used. Both simulation and field test show that the dual PN based localization scheme is robust in the low cost localization design and in UWA channels.

2. PN BASED TOA ESTIMATION SCHEME

We consider two PN based approaches in ToA estimation: single PN scheme and DPN scheme. Both single PN and DPN schemes estimate the ToA by detecting the peak index of the correlation output. In this section, we briefly review these two PN based ToA estimation methods.

2.1. Single PN scheme. The transmitted signal in the single PN scheme is depicted in Fig. 1. A PN sequence of length N_{S1} is added before the message payload as a preamble, which is used for ToA estimation. Besides, a length N_{S2} guard interval is inserted between the the preamble and the payload to prevent the Inter-Block Interference (IBI).
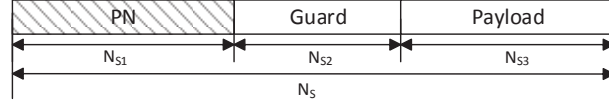

Figure 1. Transmitted signal frame in the single PN scheme.

We calculate the cross-correlation of the received single PN signal and the local PN sequence to obtain the ToA estimation. Let $x_{sb}(t)$ be the baseband PN of the transmitted signal with pulse shaping. The transmitted passband signal is expressed as

$$x_{sp}(t) = Re\{x_b(t)e^{j2\pi f_c t}\} \tag{1}$$

where $j = \sqrt{-1}$, f_c is the carrier frequency at the transmitter, and $Re\{\}$ is the real part of a complex variable. Let the bansband channel be $h_b(t)$, which includes an unknown fraction phase delay, and the passband channel is then

$$h_p(t) = Re\{h_b(t)e^{j2\pi f_c t}\} \tag{2}$$

At the receive side, the received signal

$$y_{sp}(t) = x_{sp}(t) \otimes h_p(t) + \eta_p(t) \tag{3a}$$

$$= Re\{x_b(t)e^{j2\pi f_c t}\} \otimes h_p(t) + \eta_p(t) \tag{3b}$$

$$= Re\{x_b(t) \otimes h_b(t)e^{j2\pi \Delta f_c t}e^{j2\pi f_c' t}\} + \eta_p(t) \tag{3c}$$

where $\eta_p(t)$ is the additive Guassian noise, the operator $\otimes$ represents the convolution operation, $\Delta f_c = f_c - f'_c$ is the carrier frequency offset caused by the low-cost localization system, f'_c is the coherent carrier frequency at the receiver, and let $\tilde{x}_b(t) = x_b(t) \otimes h_b(t) e^{j2\pi \Delta f_c t} + \eta_b(t)$ be the received complex baseband equivalent signal, where $\eta_b(t)$ is the baseband noise.

The passband local single PN signal with the coherent carrier frequency is

$$x_{sl}(t) = Re\{x_b(t) e^{j2\pi f'_c t}\} \tag{4}$$

The correlation of the local PN signal and the received PN signal is calculated as

$$R_s(t) = x_{sl}(t) \odot y_{sp}(t) \tag{5a}$$

$$= Re\{[x_b(t) \odot \tilde{x}_b(t)] \cdot [e^{j2\pi f'_c t} \odot e^{j2\pi f'_c t}]\} \tag{5b}$$

$$= Re\{R^S_{x\tilde{x}}(t) \cdot R_{c'c'}(t)\} \tag{5c}$$

where the operator $\odot$ represents the correlation operation, the operator $\cdot$ represents the multiplication, $R^S_{x\tilde{x}}(t) = x_b(t) \odot \tilde{x}_b(t)$ is the cross-correlation of the local PN and the transmitted single PN signal with frequency offset and multipath channel, and $R_{c'c'}(t) = e^{j2\pi f'_c t} \odot e^{j2\pi f'_c t}$ is the auto-correlation of the carrier wave. Note that the CFO and channel effects are included in $R^S_{x\tilde{x}}(t)$.

2.2. DPN scheme. The data structure of DPN scheme is described in Fig. 2. The DPN frame has two identical PN sequences, instead of one PN sequence, as the frame preamble. A guard interval of N_{D2} is inserted between two PN segments to prevent IBI. These two PN segments in the preamble are used to estimate the arrival time of a frame by calculating their cross-correlation.

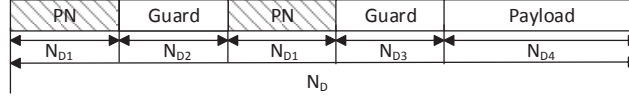| PN	Guard	PN	Guard	Payload
N_{D1}	N_{D2}	N_{D1}	N_{D3}	N_{D4}

N_D

Figure 2. Transmitted signal frame of the DPN scheme.

The passband transmitted signal is expressed as

$$x_{Dp}(t) = Re\{[x_{D1}(t) + x_{D1}(t - t_2)]e^{j2\pi f_c t}\}. \tag{6}$$

where $t_2 = (N_{D1} + N_{D2})T_0$ (T_0 is the symbol duration), and $x_{D1}(t)$ represents the first PN sequence with pulse shaping. The received signal at passband is

$$y_{Dp}(t) = x_{Dp}(t) \otimes h_p(t) + \eta_p(t)$$
$$= Re\{[x_{D1}(t) + x_{D1}(t-t_2)] \otimes h_b(t)e^{j2\pi f_c t}\}$$
$$+ \eta_p(t) \tag{7}$$

The received signal is saved in memory and the first segment is delayed by t_1. Assuming the channel experienced by the two segments is the same, then the correlation between the two PN segments is calculated as

$$R_D(t) = [Re\{x_{D1}(t - t_1) \otimes h_b(t)e^{j2\pi f_c t}\} + \eta_p(t)]$$
$$\odot [Re\{x_{D1}(t - t_2) \otimes h_b(t)e^{j2\pi f_c t}\} + \eta_p(t)] \tag{8a}$$
$$= R_e\{R_{xx}^D(t) \otimes R_{hh}(t) \cdot R_{cc}(t)\} + R_\eta(t) \tag{8b}$$

where $R_\eta(t)$ is the correlation related to the noise signal, $R_{xx}^D(t) = x_{D1}(t - t_1) \odot x_{D1}(t - t_2)$ with $t_1 = t_2$ is the cross-correlation of the two baseband PN segments of the transmitted single, $R_{hh}(t) = h_b(t) \odot h_b(t)$ is the auto-correlation of the baseband channel. Note $R_{cc}(t) = e^{j2\pi f_c t} \odot e^{j2\pi f_c t}$.

From equation (8b), we find that the cross-correlation of the two PN segments in the received signal actually focuses the multipath signal energy into a smaller number of taps, which increases the reliability of the ToA estimation in UWA channels. Moreover, the CFO would has no influence on the correlation because both segments experience the same CFO.

3. SIMULATION RESULTS

In this section, we use simulation to evaluate the performances of single PN and DPN schemes for ToA estimation under CFO and UWA multipath delay. The PN sequences were generated using maximal linear feedback shift registers (MLS), termed as m-sequence. For length-m registers, it produces a sequence of $(2^m - 1)$ bits. We added one bit of zero at the end of the m-sequence so that the PN length is 2^m bits.

3.1. The method of evaluate correlation property. Since the ToA is measured through detecting the peak time index of the cross-correlations of PN sequences, we propose a method to measure the correlation performance of both the single PN and DPN schemes. If the correlation is conducted without signal distortions, we consider it as the reference correlation C_0 and its peak time index as the reference peak index P_T. We set a window centered at time index P_T for correlation observation. The window size W_S should be large enough to include the main lobe of the reference correlation curve so that the main energy of the correlation is contained in this window. Fig. 3 gives a correlation output of two PN sequences with a window centered at P_T. Besides, the section of a correlation curve occupying the window is termed as C_W. We calculate the energy of C_W as

$$P_{CW} = \sum_{k=P_T-W_S/2}^{P_T+W_S/2} R_y^2[k] \tag{9}$$

Where $R_y[k]$ is the correlation after sampling. The total energy of the correlation output is expressed as

$$P_C = \sum_{k \subseteq K} R_y^2[k] \tag{10}$$

where K represent the whole set of time indexes of the correlation curve. The correlation performance metric S_C is measured by

$$S_C = \frac{P_{CW}}{P_C} \tag{11}$$

where S_C is the ratio of the energy in the window over the whole energy of the correlation output. And let S_{C0} represents the reference correlation C_0 performance, over which other S_C will be evaluated. The correlation performance relative to the reference correlation is expressed as

$$R_C = \frac{S_C}{S_{C0}} \tag{12}$$

When the correlation performance gets worse, the main lobe spreads or the peak index drifts from P_T, which lower P_{CW} and R_C. Note that the R_C value will vary with different W_S. When we evaluate the correlation performance in different situations, W_S should keep being identical. In our simulations, we set W_S equals to two bit duration, which contains and only contains the main lobe of the reference correlation curve. If only one distinct peak can be observed in a correlation curve, we consider it as reliable for ToA estimation. According to this criterion We can set a threshold value of R_C to evaluate the reliability of the correlation for accurate ToA estimation. Any correlation output with R_C larger than the threshold is considered as good enough to estimate ToA.

3.2. Carrier frequency offset (CFO) effect. Fig. 4 shows the correlation performance of two single PNs with different CFOs. The multipath channel and noise are not considered in this simulation. The case number represents different cases. Case1: $N_{S1} = 32$ bits; case2: $N_{S1} = 64$, case3: $N_{S1} = 1284$; case4: $N_{S1} = 256$ bits. Note that R_C is '1' when there is no CFO and decreases with increasing CFO. We set the threshold $R_C = 0.2$ by analyzing the correlation outputs in our simulations. For example, the correlation outputs with CFO=1800 PPM are not reliable because it's R_C is smaller than 0.2. Besides, from Fig. 4 we find the longer PN sequences are more sensitive to CFO.
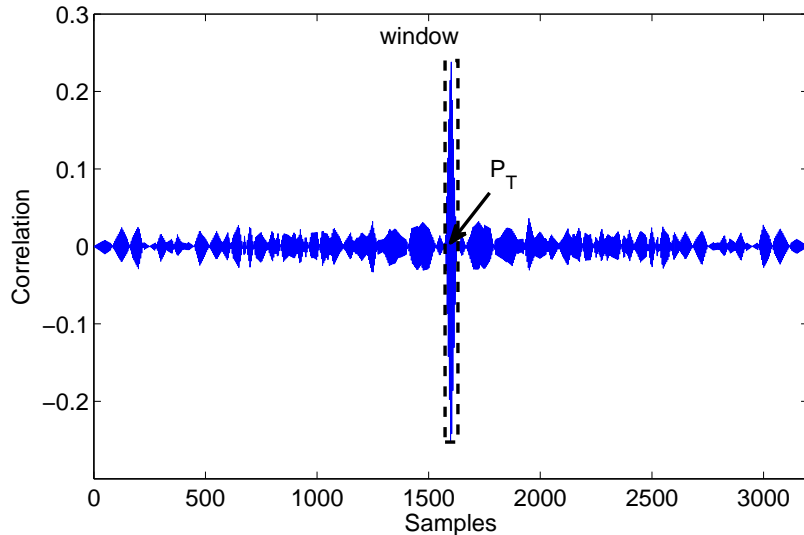
Figure 3. Correlation of single PN scheme with CFO=200 PPM, PN length=64 bits.

The correlation performance of DPN scheme with CFO is demonstrated in Fig. 5. The cases presented in Fig. 5 has the same PN lengths as the cases in Fig. 4, and the guard length is set as 200 bits for all cases. Obviously, the DPN correlations almost do not change with different levels of CFOs, almost stay at the value of '1'. Therefore, we conclude that the CFO would not affect the correlation output in the DPN scheme.
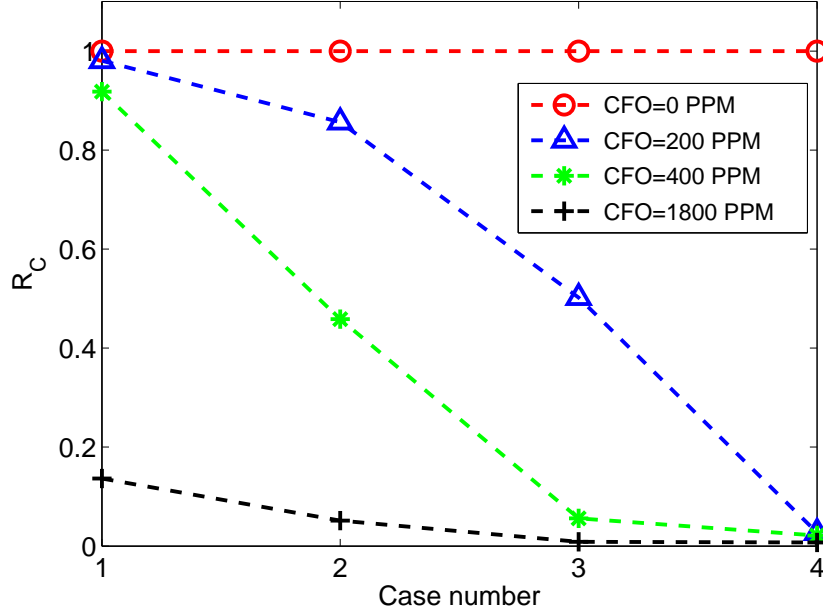
Figure 4. Correlation performance of single PN scheme with CFO.

3.3. Multipath channel effect. To evaluate the multipath effect on the PN based ToA estimation, we adopted an estimated channel from field experiment shown in Fig. 6 in our simulation. This channel is very tough for ToA estimation, as it exhibits severe multipath effect and the first path is not with the strongest energy. Note in the following simulation, both CFO and noise are not considered. Fig. 7 depicts the correlation performance of single PN with multipath delay. Compared with the correlation output without multipath channel, the reliability of the correlation R_C under multipath channel decreases to be below 0.2. Therefore, the multipath delay has significantly influence on the correlation performance of single PN scheme.

The correlation performance of DPN scheme under multipath channel is shown in Fig. 8. Note that although R_C is reduced with multipath channel comparing with the R_C without channel, it is still good enough to get the accurate ToA estimation,
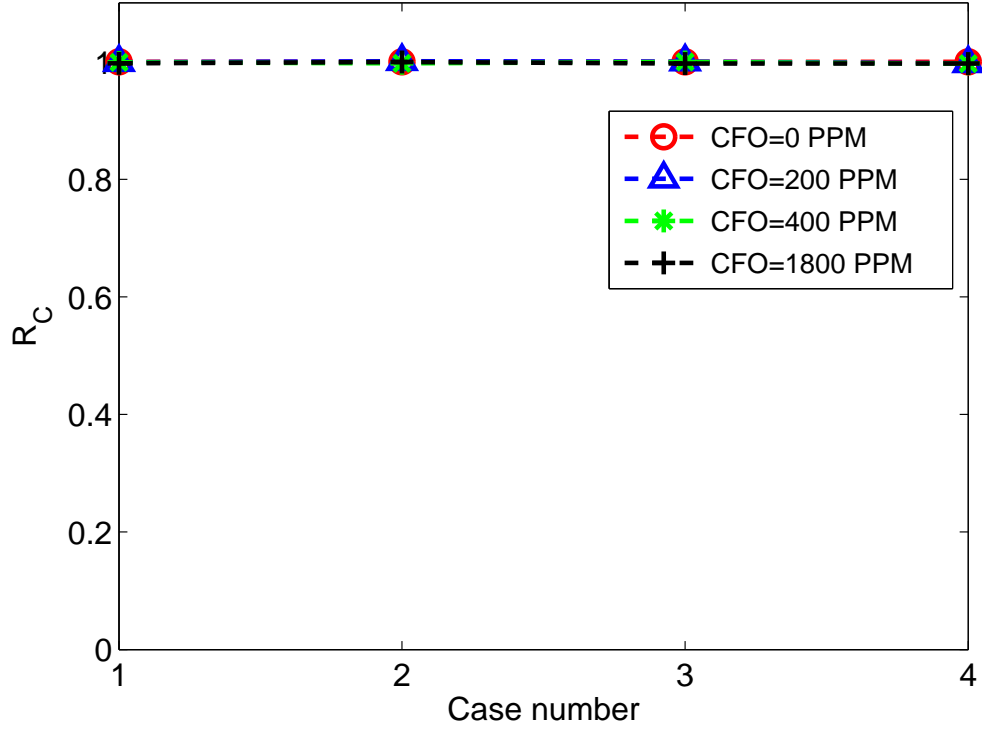
Figure 5. Correlation performance of DPN scheme with CFO.

because all the R_C is higher than the threshold we set. Thus, the ToA estimation based on the DPN signal can efficiently combat the multipath delay effect in the UWA channels.

4. EXPERIMENT RESULTS

A hardware test-bed was designed to verify the PN based localization schemes. The circuit board serves as a transceiver in the acoustic communication, forming a node in UWSN. To reduce the cost of the test-bed, We chose the low power dissipation and cheap MCU, Texas Instrument MSP430F5529, which contains a 12-bit analog to digital converter (ADC12) module. The conversion results of the ADC12 are restored in the SRAM of MCU. A cheap crystal oscillator CSTCR4M00G15L99 is used as the source of the main clock in MCU, termed as $MCLK$. Its price is US \$0.7 per unit,
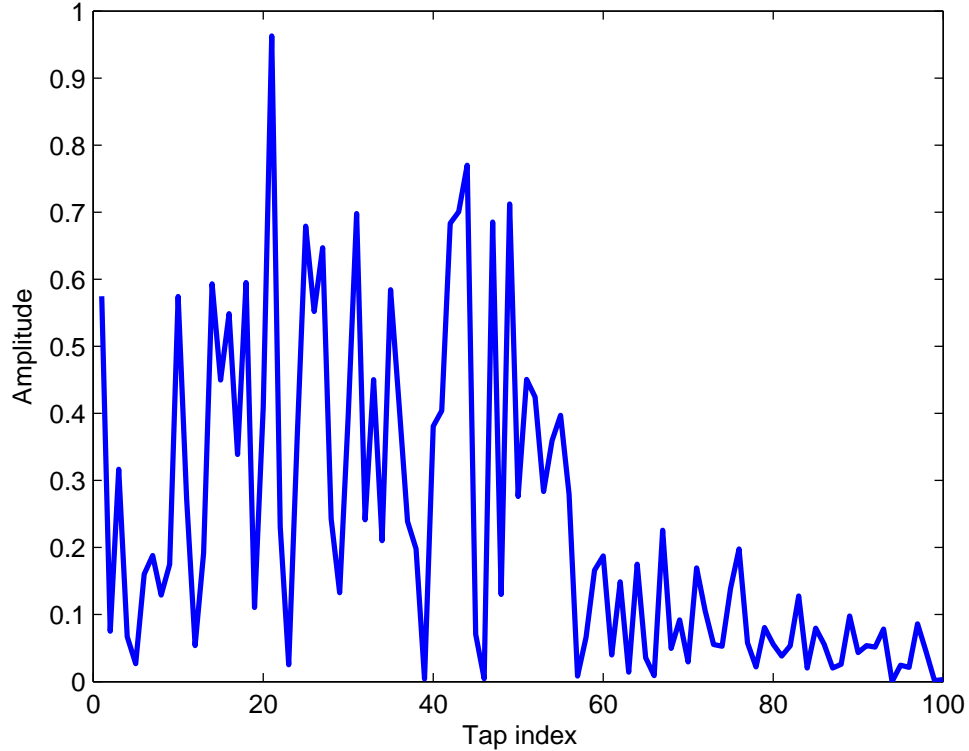
Figure 6. Estimated channel impulse response with to-sampling, from $T_X 3$ to $R_X 1$.

which is extremely cheap comparing with the atomic clock that is commonly used in underwater localization. Even the oversize oscillator used in [2] is US \$3.5 per unit. Meanwhile, the low-cost design has some disadvantages. First, The SRAM in the MCU is limited. Thus, We set the ADC output to be left aligned. That is we only save the higher 8 bits of out the 12-bit ADC results and throw the lower 4 bits away, reducing the result resolution while doubling the available memory in MCU. Second, the oscillator CSTCR4M00G15L99 has high frequency offset up to 1800 PPM. The main draw back of the hardware test-bed is the high CFO.

We conducted a field experiment to test the PN based ToA estimation schemes on the low-cost test-bed. The experiment field was at the Pine Lake, Rolla, MO, in November 2015. The lake and area are shown in Fig. 9, where the wooden bridge
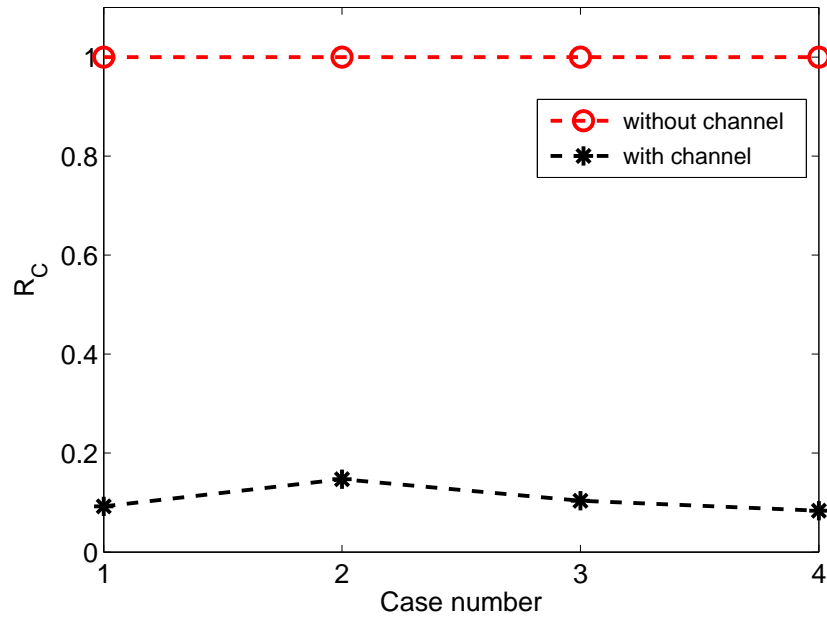
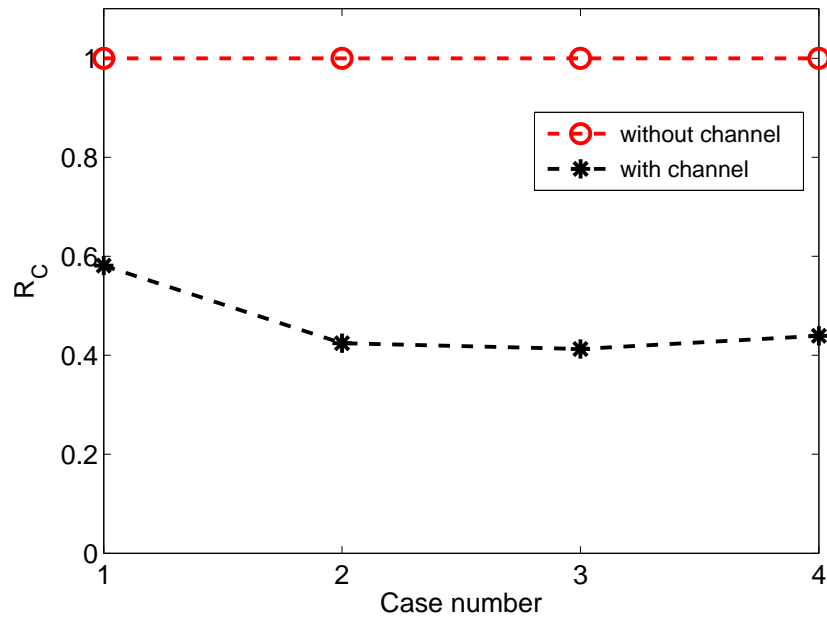Figure 7. Correlation performance of single PNs with multipath channel.

Figure 8. Correlation performance of DPN scheme with multipath channel.

runs across the island and the side of the lake. We placed four receivers $R_X 1$ to $R_X 5$ around the wooden bridge and four transmitters $T_X 1$ to $T_X 4$ on the bridge, which are shown in Fig. 9.
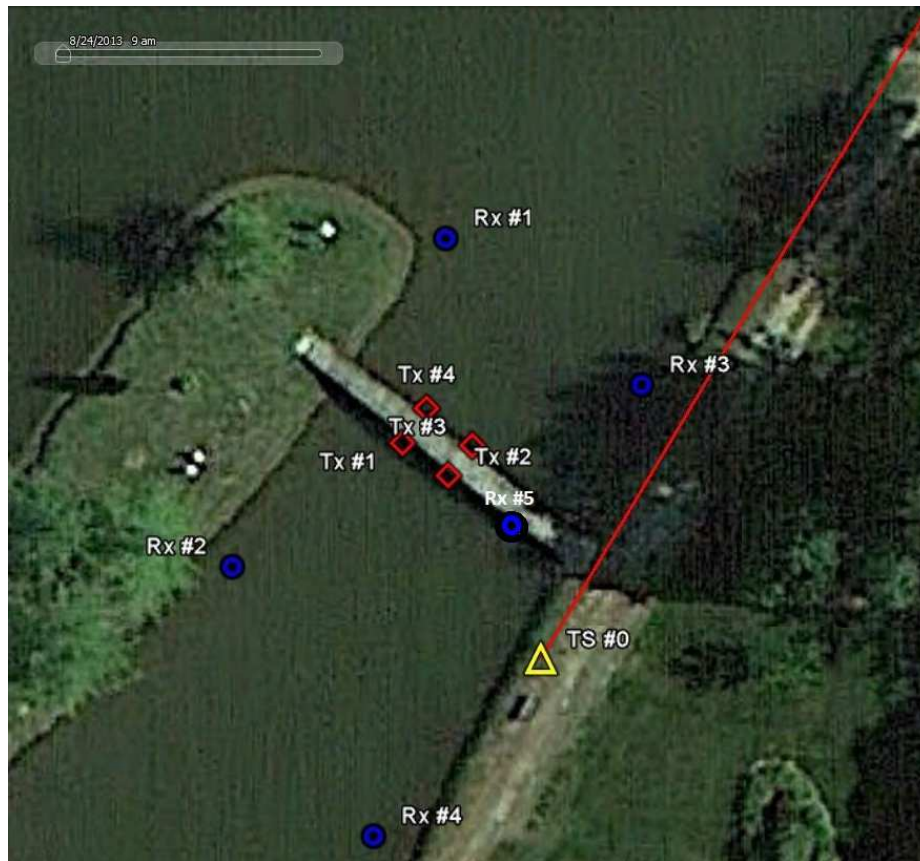
Figure 9. Experiment spot for the field test at Pine Lake, Rolla, MO.

Fig. 10 shows the correlation performance of the the local PN and received single PN signal with $N_{S1} = 128$ bits, at R_X1, T_X3, at the $10th$ second. As there is no distinct peak observed in Fig. 10, We are unable to detect the correct peak location. Note that the ToA estimation in Fig. 10 should the difference of a possible distinct peak index in this curve and the index of 5000. At the same time slot and location, the correlation output of the DPN scheme shown in Fig. 11 has only one distinct peak. And the ToA estimation in this figure is the peak index. Therefore, the accurate ToA estimation is achieved with the DPN based scheme.
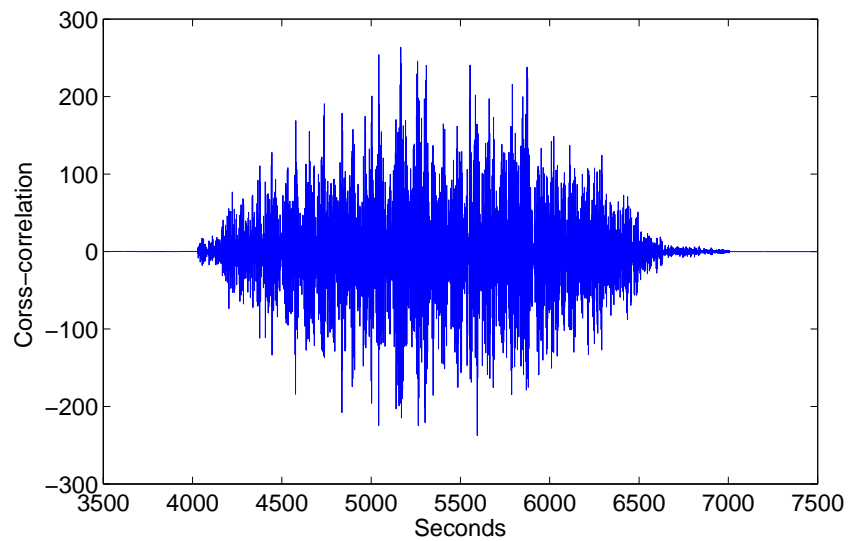
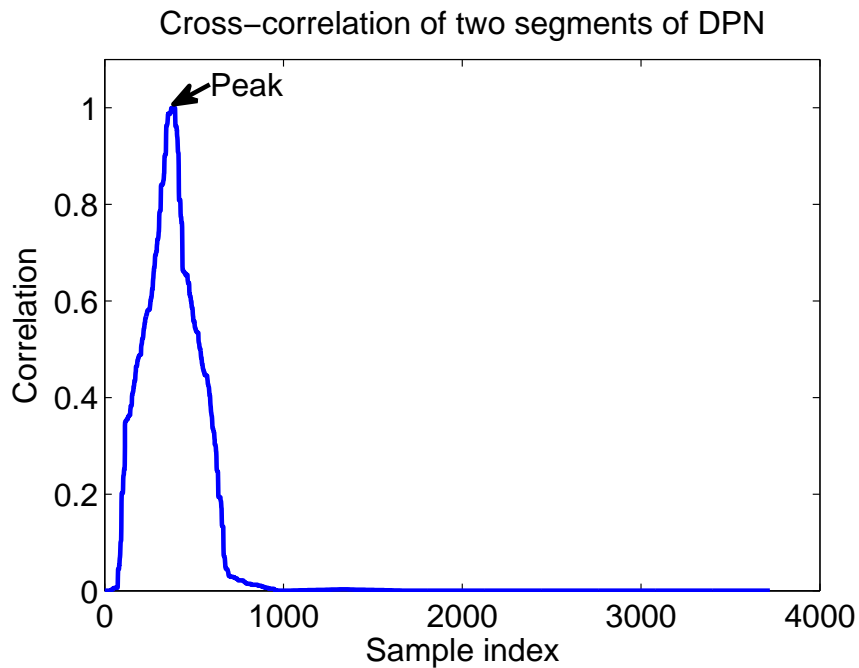Figure 10. Cross-correlation of local PN and received single PN.

Figure 11. Cross-correlation of two PNs in the DPN frame.

5. CONCLUSION

This paper compares two PN based localization schemes on a low-cost hardware system for ToA estimation in UWA localization. The simulation and field experiment results show single PN approach is sensitive to the UWA channel multipath

delay, and also requires higher frequency precise of the system clock. In contrast, the DPN scheme can effectively combat the severe multipath effect in UWA channel. Moreover, CFO in our low-cost hardware test-bed has no influence to the DPN scheme. Therefore, the DPN scheme is more promising for the low cost localization system in severe UWA environments.

6. ACKNOWLEDGMENT

REFERENCES

[1] M. Erol-Kantarci, H. T. Mouftah, and S. Oktug, "Localization techniques for underwater acoustic sensor networks," *Communications Magazine, IEEE*, vol. 48, no. 12, pp. 152–158, 2010.

[2] Y. R. Zheng, Z. Yang, J. Hao, and P. Han, "Hardware implementation of underwater acoustic localization system for bridge scour monitoring," in *Oceans-San Diego, 2013.* IEEE, 2013, pp. 1–6.

[3] H.-P. Tan, R. Diamant, W. K. Seah, and M. Waldmeyer, "A survey of techniques and challenges in underwater localization," *Ocean Engineering*, vol. 38, no. 14, pp. 1663–1676, 2011.

[4] H. Li, Y. He, X. Cheng, H. Zhu, and L. Sun, "Security and privacy in localization for underwater sensor networks," *Communications Magazine, IEEE*, vol. 53, no. 11, pp. 56–62, 2015.

[5] M. Stojanovic and J. Preisig, "Underwater acoustic communication channels: Propagation models and statistical characterization," *Communications Magazine, IEEE*, vol. 47, no. 1, pp. 84–89, 2009.

SECTION

2. SUMMARY AND CONCLUSIONS

This dissertation proposes two novel magnetic induction (MI)-based localization methods in wireless sensor networks, which can be applied in some challenging environments such as underground, underwater, inside of animals, and indoor. A close-form formula of the transmission distance is derived in this dissertation. Taking advantage of magnetic field measurements of the tri-directional coil at each node, this method is able to locate sensor nodes with arbitrary orientations and positions in the 3-D space, only assisted with two anchor nodes. Assuming each anchor node sequentially transmits the communication signal by the three orthogonal Tx coils in a tri-directional structure, and the sensor node receives the signals at the three orthogonal Rx coils simultaneously, the communication distance and the polar angles of transmission are estimated in a local coordinate system of the anchor node. These estimates from the two anchor nodes yield two sets of 8 possible locations of the sensor node. Then, a rotation matrix (RM) between the transmitter and receiver is derived to narrow down to two possible location vectors with the opposite directions in each anchor node. Finally, we use the maximum likelihood method to estimate the accurate location from the two sets of two location vectors. Another is distance-based method that finds the minimum distance between nodes in two local coordinates system. The pair of nodes with minimum distance are used to locate the sensor node. Numerous simulations show the proposed RM-based method can reach high localization accuracy under large measurement errors. Simulation results also

prove the RM-based method has higher accuracy in terms of transmission distance estimation than the wide-used RSSI model. On the other hand, the distance-based method xhibits less computational complexity and is faster.

This dissertation also proposes a novel node localization method based on acoustic communications for underwater wireless networks (UWSNs) in 2-D and 3-D spaces, respectively, where only a small number of anchor nodes are available. The proposed scheme estimates distances from anchor nodes to sensor nodes via multi-hop propagations with the help of angle of arrival (AoA) measurements. By forwarding distances hop-by-hop through the wireless network, the distance estimations can be flooded to the whole network even if the network is sparse. Once a sensor node obtains distance estimates from at least three (in 2-D) or four (3-D) anchor nodes, it can compute its own location by the trilateration algorithm. In contrast to existing multi-hop methods such as DV-hop, DV-distance, Euclidean method, Cosine-law method, and Distance-based method, our proposed method uses rotation matrices between neighboring nodes to estimate Euclidean distances to anchor nodes. Therefore, the proposed method can improve localization accuracy significantly. Simulation results show that our method can achieve high distance and localization accuracy. Besides, our methods can reach the same high localization coverage as DV-hop, DV-distance, the Distance-base method, and the Consine-law method in the 2-D space, even though the localization coverage gets relatively lower in the 3-D space.

This dissertation investigates the performances of single pseudo-noise (PN) and dual PN (DPN) sequences for time of arrival (ToA) estimation in underwater acoustic (UWA) localization. ToA is widely used to estimate distance in UWA localization. The accuracy of ToA estimates is crucial to localization accuracy. The single PN scheme calculates the correlation of a local PN sequence and the received PN signal to estimate the ToA. The DPN scheme calculates the cross correlation of the two received PN segments in one signal frame to estimate the ToA. The simulation and

field experiment results show that the single PN approach is sensitive to the UWA channel multipath delay and also requires higher frequency precise of the system clock. In contrast, the DPN scheme can effectively combat the severe multipath effect in UWA channel. Moreover, CFO in our low-cost hardware test-bed has no influence to the DPN scheme. Therefore, the DPN scheme is more promising for the low-cost localization system in severe UWA environments.

APPENDIX

PUBLICATION LIST

[1] H. Huang, Y. R. Zheng, "Node Localization with AoA Assistance in Multi-hop Underwater Sensor Networks", *Elsevier Ad Hoc Networks.*, Jul. 2017. [Submitted]

[2] H. Huang, Y. R. Zheng, "3-D Localization of Wireless Sensor Nodes Using Near-Field Magnetic-Induction Communications", in *Elsevier Physical Communication*, May. 2017. [Submitted]

[3] H. Huang, Y. R. Zheng, "Node Localization in 3-D by Magnetic-Induction Communications in Wireless Sensor Networks", in *Proc. MTS/IEEE OCEANS*, Anchorage, USA, Sep. 18-21, 2017. [Accepted]

[4] H. Huang, Y. R. Zheng, "AoA assisted localization for underwater Ad-Hoc sensor networks", in *Proc. MTS/IEEE OCEANS*, Monterey, USA, Sep. 19-21, 2016. pp. 1-6.

[5] H. Huang, Y. R. Zheng, and W. Duan, "Pseudo-Noise Based Time of Arrival Estimation for Underwater Acoustic Sensor Localization", in *Proc. MTS/IEEE OCEANS*, Shanghai, China, Apr. 11-14, 2016. pp. 1-6.

REFERENCES

[1] M. Garcia, S. Sendra, M. Atenas, and J. Lloret, "Underwater wireless ad-hoc networks: A survey," *Mobile ad hoc networks: Current status and future trends*, pp. 379–411, 2011.

[2] V. Chandrasekhar, W. K. Seah, Y. S. Choo, and H. V. Ee, "Localization in underwater sensor networks: survey and challenges," in *Proceedings of the 1st ACM international workshop on Underwater networks*. ACM, 2006, pp. 33–40.

[3] Z. Zhou, Z. Peng, J.-H. Cui, Z. Shi, and A. Bagtzoglou, "Scalable localization with mobility prediction for underwater sensor networks," *IEEE Transactions on Mobile Computing*, vol. 10, no. 3, pp. 335–348, 2011.

[4] M. Erol, L. F. M. Vieira, and M. Gerla, "Auv-aided localization for underwater sensor networks," in *Wireless Algorithms, Systems and Applications, 2007. WASA 2007. International Conference on*. IEEE, 2007, pp. 44–54.

[5] Z. Zhou, J.-H. Cui, and S. Zhou, "Localization for large-scale underwater sensor networks," in *International Conference on Research in Networking*. Springer, 2007, pp. 108–119.

[6] D. Niculescu and B. Nath, "Ad hoc positioning system (aps)," in *Global Telecommunications Conference, 2001. GLOBECOM'01. IEEE*, vol. 5. IEEE, 2001, pp. 2926–2931.

[7] Z. Zhu, W. Guan, L. Liu, S. Li, S. Kong, and Y. Yan, "A multi-hop localization algorithm in underwater wireless sensor networks," in *Wireless Communications and Signal Processing (WCSP), 2014 Sixth International Conference on*. IEEE, 2014, pp. 1–6.

[8] N. H. Will and J. Schiller, "Distance-based distributed multihop localization in mobile wireless sensor networks," *8th GI/ITG KuVS Fachgesprch Drahtlose Sensornetze (FGSN09)*, vol. 34, 2009.

[9] E. Slottke and A. Wittneben, "Accurate localization of passive sensors using multiple impedance measurements," in *Vehicular Technology Conference (VTC Spring), 2014 IEEE 79th.* IEEE, 2014, pp. 1–5.

[10] A. Sheinker, B. Ginzburg, N. Salomonski, L. Frumkis, and B.-Z. Kaplan, "Localization in 3-d using beacons of low frequency magnetic field," *IEEE Transactions on Instrumentation and Measurement*, vol. 62, no. 12, pp. 3194–3201, 2013.

VITA

Huai Huang received the B.S. degree in electrical engineering from Shandong University, in Jinan, China, in 2005. She received the M.S. degree in electrical engineering from Beijing University of Science and Technology, Beijing, China, in 2008. She began her Ph.D. study in August 2014 at the Department of Electrical and Computer Engineering at Missouri University of Science and Technology (formerly: University of Missouri-Rolla), Rolla, MO, USA. Her research interests included node localization in underwater wireless sensor networks by accoustic and MI communications. She received her Ph.D. degree in electrical engineering from Missouri University of Science and Technology in Decemeber 2017.